ISSN Application No. 21799

Journal of Water Resources and Civil Engineering Technology

Volume No. 7

Issue No. 1

January - April 2023

ENRICHED PUBLICATIONS PVT. LTD

S-9, IInd FLOOR, MLU POCKET,
MANISH ABHINAV PLAZA-II, ABOVE FEDERAL BANK,
PLOT NO-5, SECTOR-5, DWARKA, NEW DELHI, INDIA-110075,
PHONE: - + (91)-(11)-47026006

Journal of Water Resources and Civil Engineering Technology

Aims and Scope

Journal of Water Resources and Civil Engineering Technology is peer reviewed journal for the presentation of original contributions and the exchange of knowledge and experience on the management of water resources. In particular, the journal publishes contributions on: Water resources assessment, development, conservation, planning and design of water resource systems; and operation, maintenance and administration of water resource systems etc.

The topics covered in this journal are:-

1. Water demand and consumption;
2. Applied surface and groundwater hydrology;
3. Water management techniques;
4. Simulation and modeling of water resource systems;
5. Forecasting and control of quantity and quality of water;
6. Economic and social aspects of water use;
7. Legislation and water resources protection

Journal of Water Resources and Civil Engineering Technology

Journal of Water Resources and Civil Engineering Technology

(Volume No. 7, Issue No. 1, January - April 2023)

Contents

Sr. No.	Articles/ Authors Name	Pg. No.
1	Application of A Groundwater Cooling System as Thermal Barrier to Establish A Comfortable Environment *– Ting- Yu Chen, Hsin- Hua Wu*	1 - 10
2	Stagnation Point Flow of Casson Fluid Over Exponentially Stretching Sheet with Variable Thermal Conductivity And Newtonian Heating *– Kartini Ahmad, Zaharah Wahid, Zahir Hanouf*	11 - 18
3	Performance of Multiple Tuned Liquid Column Dampers in Vibration Control of Structures Under Real Earthquake Excitation *– Rama Debbarma, Debasis Panda, Arka Mitra*	19 - 28
4	Response Mitigation of Structures using Liquid Column Vibration Absorber Considering Real Earthquake Ground Motions *– Debasis Panda, Rama Debbarma, Arka Mitra*	29 - 40
5	Hourly Rainfall Generation by Markov Chain Rainfall Generator *- Ujjwal Saha*	41 - 50

Application of A Groundwater Cooling System as Thermal Barrier to Establish A Comfortable Environment

[1] Ting- Yu Chen, [2] Hsin- Hua Wu

[1]Department of Landscape Architecture, National Chin-Yi University, Taichung, Taiwan

Email: [1]tychen@ncut.edu.tw, [2]selina2751@gmail.com

ABSTRACT

Taiwan is limited in space with dense population, and is located in sub-tropical region with high ambient temperature and humidity. The development of buildings must consider issues on the climatic condition, population, and land usage. In recent years, changes of social structure and nature of work cause people to stay indoors longer. Thus, pursuing a comfortable indoor working and living environment is become an important research topic. Thermal barrier technologies have become an important energy-saving for space heating and cooling of residential and commercial buildings in many countries. Building energy efficiency can be improved by implementing either active or passive energy efficient strategies. Improvements to heating, ventilation and air conditioning systems etc. can be categorized as active strategies, whereas, improvements to building envelope elements can be classified under passive strategies. Using groundwater cooling system as thermal barrier is one of the effective passive strategies. Groundwater cooling system is composed of galvanized iron pipes located inside of walls. Fluid flows inside the pipes and then supply constant cooling temperature. In the study, system using of groundwater as renewable energy source for pipes cooling. The groundwater at depth of more than 5 meters below the surface has constant temperature year round. Lower temperature groundwater would cool the pipes of system by heat exchange process to achieve the cooling effect of wall. In this research, cooling wall system was evaluated to reduce the thermal transfer from sunlight into the buildings, thus reducing the electricity consumption needs for air conditioning of the buildings.

Keywords: Groundwater cooling system、Thermal barrier、passive strategies.

I. INTRODUCTION

Under the effects of global warming and the rapidly exhausted fossil fuels in the 21st century, the renewable energy source and clean energy are proposed by many experts and scholars, hoping to reduce the environmental impact. The subterranean heat and cold resources are one of the projects discussed, making them into substitute energy and the practical application of research have become the research objective of renewable energy source (Heng and Rybach, 2005; Okubo et al., 2003; Taniguchi et al., 1998; Taniguchi et al., 2005). The underground temperature distribution is used to evaluate the climate change in the past, the groundwater temperature is derived not only from transfer, but also from the convection with surface water (Miyakoshi et al., 2003). Generally speaking, the groundwater temperature remains constant, but some documents indicate that the groundwater varies with woodcutting, urbanization even climate change (Taniguchi et al., 2005). The groundwater temperature is obtained generally by setting borehole or deep well, the Water Resources Agency, Ministry of

Economic Affairs, has located deep and shallow wells in various places of Taiwan to survey hydrogeological information. At present, some documents have indicated that using geothermal and underground cooling systems as alternative energy sources is feasible (Heng and Rybach, 2005; Grant,2012; Antonio and Matteo,2013; Ampofo et al., 2011). The (groundwater) temperature over 5 m below the surface almost remains constant all the year round, as the depth increases, the temperature is lower than the air temperature in summer daytime, the water temperature in the depth of ground is enough to warm the house in winter. If the underground "cold" and "heat" resources can be used properly, the thermal circulation indoor temperature control system can be built for cooling/thermal insulation.

II. EXPERIMENT METHOD

The underground cold/geothermal application depends on groundwater temperature stability and flow velocity. A constant groundwater temperature can provide cooling source or heating source for the building walls effectively, and a stable groundwater velocity decides whether the heat source can diffuse in time, so as to keep the heat exchange stable. In the pilot test, the influence of detailed pipe system design and the recirculation system on the variation of groundwater temperature is studied using concrete testing walls. The pilot-test system consists of heat exchanger, concrete testing sample, water recirculation pump, solar energy plate and the monitoring system as shown in Fig. 1.

Fig. 2 shows the computer model using CFD (Computational fluid dynamics) of the testing wall plate module to simulate temperature variations of the concrete wall, metal pipes and the groundwater flowing in the metal pipe. Denser grids are provided for locations where more vigorous heat exchange is expected so that the simulation results represent the real situation. As shown in Fig. 3, the results using 30 w to 250 w cells indicate that the grid with 150 w cells is neither divergent nor convergent with stable and satisfactory simulation results; this grid is used for conducting all subsequent simulations based on 0.1 m3/h of 19 groundwater.

Fig. 1 Installation of the pilot testing concrete wall plate

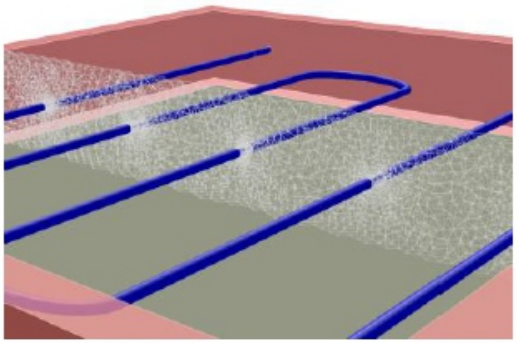

Fig. 2 schematic diagram of the concrete wall plate embedded with S-shaped groundwater cooling pipe system

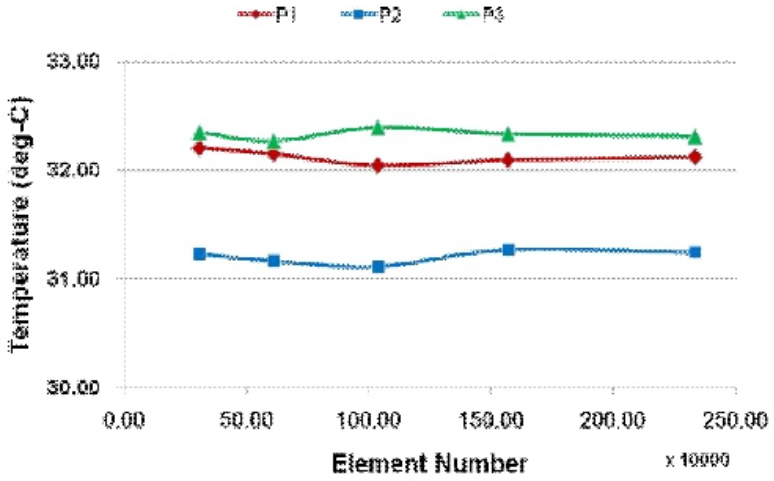

Fig. 3 Detailed establishment of grids

The recorded parameters of pilot test will be used as reference, combined with the simulation program Fluent-CFD (Computational fluid dynamics) to simulate the temperature transfer among the sun, the concrete wall, metal pipes and the groundwater flowing in the metal pipe. The CFD is an actively developed science, theoretically it studies and describes various linear equations of fluid. In engineering applications, the purpose is to use the computer numerical calculation to prove the test results and to improve the design. The simulation of natural ventilation of buildings was studied since the 1970's. In recent years, as the computer arithmetic capability is enhanced greatly, the computer simulation program of CFD is used to simulate the thermal environment to predict the effect of sun illumination on the buildings. This study uses finite difference to control volume approximate numerical method, and uses the assumed computing mesh to analyze the distribution of velocity field and temperature field in the site space. The "grid system" divides the region to be calculated into appropriate grids, each grid contains a computing point, and a set of continuity equations for the mass, energy and temperature field in the site space. The "grid system" divides the region to be calculated into appropriate grids, each grid contains a computing point, and a set of continuity equations for the mass, energy and momentum conditions of each grid is used for iterative operation. Different grids are used for model grid

independence test in the simulation process. A point of the model is selected as reference point , different heights are selected for grid test analysis. There are seven groups of analyses for grid test analysis. This study simulates the convection heat transfer instantaneously, the time average of physical characteristics is discussed through quasi-static process, so as to obtain highly reliable results. The governing equation for the flow field is expressed as follows:

$$\rho\frac{\partial\bar{V}}{\partial t}+\rho(\bar{V}\cdot\nabla)\bar{V}=-\nabla P+\rho\bar{g}+\mu\nabla^2\bar{V} \quad (1\text{-}1)$$

The pressure term, gravity term and shear force term of object are on the right of equal sign.

$$\rho C_p\frac{\partial T}{\partial t}+(\bar{V}\cdot\nabla)\rho C_pT=\nabla\cdot(k\nabla T)+\mu\Phi+\dot{q} \quad (1-2)$$

The thermal diffusion, viscosity diffusion and heat source term of object are on the right of equal sign.

$$\rho=\frac{p_{op}+p}{\frac{R}{M_w}T} \quad (1-3)$$

T：Temperature；ρ：Density；Cp：Specific Heat；q ：Heat source (mean solar radiation) ；R：Gas constant；MW：molecular weight of gas.

Where -ÑP is the pressure force; $\rho\bar{g}$ s the gravity force; $\mu\nabla^2\bar{V}$ s the shearing force; $\nabla\cdot(k\nabla T)$ is the conduction dissipation; μΦ is the Viscous dissipation; and •q is the Heat generation.

III. RESULTS AND DISCUSSION

3.1. Ambient temperature analysis and monitoring

According to long-term monitoring of onsite groundwater temperature, the groundwater temperature remains stable in various months, the winter and summer have slight effect on the groundwater temperature. The temperature of the water near the surface rises in summer, but the difference is slight. The analysis of quality of groundwater (including alkalinity, iron ion and turbidity which are likely to influence the heat exchange condition) shows that the analyzed water alkalinity is 124 mg CaCO3/L, the iron ion concentration is lower than the instrument detection limit and the water quality item nutritive salt, the concentration is in the reasonable range, it is unlikely to scale influencing the temperature exchange. The groundwater heat exchanger experiment shows that the groundwater temperature rises obviously in the daytime from 20 to 25-27, and falls to 21-22 at night, meaning the wall temperature influences the groundwater through the pipeline, increasing its temperature, but the heat is removed with water flow, not accumulated in the well. In terms of weather environment, the research time is July of summer, the daily mean temperature is 29.1 in Taichung in summer, the maximum monthly mean

temperature of July is 35.3, the minimum temperature is 23.8, the maximum instantaneous wind speed is 11.2m/s, and the average wind speed per 10 minutes is 5.2m/s.

3.2. Wall cooling circuit simulation analysis

In the pilot test, the concrete is combined with pipeline for experiment, so as to evaluate how the groundwater takes away the heat inside the wall transferred from sun illumination to the wall after the groundwater flows through the pipeline. Four conditions are evaluated, which are the thermal effects of 2, 4, 6 and 8 crooked pipelines in the wall (Fig. 4). Dense grids are located in the junction where the heat exchange is violent, so that the simulation results are closer to the actual situation. The simulated flow rate is set as 0.1 m3/h for the groundwater cooling simulation analysis, the imported groundwater temperature is set as 19. The analysis and discussion are described below:

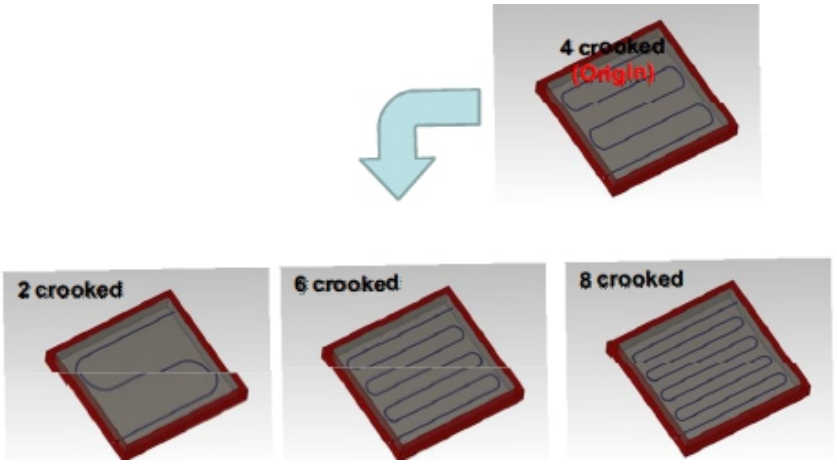

Fig. 4 2, 4, 6 and 8 crooked pipelines in the wall

3.2. Wall cooling circuit simulation analysis

The sectional view of the cooling wall is shown in Figure 5 The section LH approaches the outer wall, L0 is the section the groundwater cooling pipe goes through, LL is close to the inner wall near the interior; LH and LL sections are 5 cm away from the intermediate cooling pipeline.

a. 2 crooked pipeline through the wall

When the groundwater at 19 flows through the wall at 0.1 m3/h, the outer wall (Section LH) is exposed to the sun, its temperature rises gradually (Figure 6), the temperature is higher than 40. However, under the effect of the cooling pipeline, the temperature near the pipeline falls to 36; the temperature between pipelines rises to 39. The Section L0 shows large temperature difference, the temperature near the pipeline is 19, the temperature between pipelines rises to 34. The section near the inner wall (Section LL) has slight temperature change, the temperature near the pipeline is 28, the temperature between pipelines is about 30.

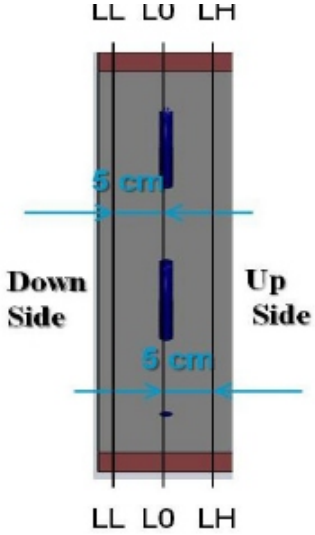

Fig.5. the cross-sections for the cooling wall

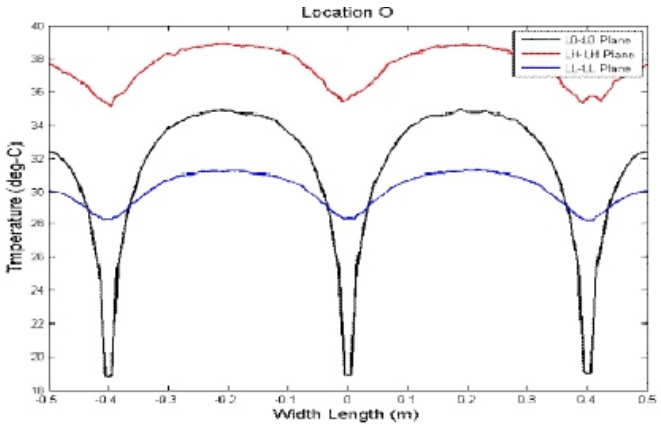

Fig. 6 Distribution of thermal transportation at the cross- sections for the 2-lap crooked pipe layout

b. 4 crooked pipeline through the wall

The layout of 4 crooked pipeline is initial pilot test planning, the simulation factors are found by onsite wall setup, the error value can be corrected, and the correct simulation planning can be found. Therefore, the simulation result is identical with the actual monitoring value (Figure 7). The outer wall (Section LH) is exposed to the sun, the maximum temperature is 38 in the wall between pipelines, the temperature near the cooling pipeline falls to 36. The Section L0 has large temperature difference, the temperature near the pipeline is 19, that between pipelines rises to 32. The section near the inner wall (Section LL) has slight temperature change, the temperature near the pipeline is 28, that between the pipelines is about 30.

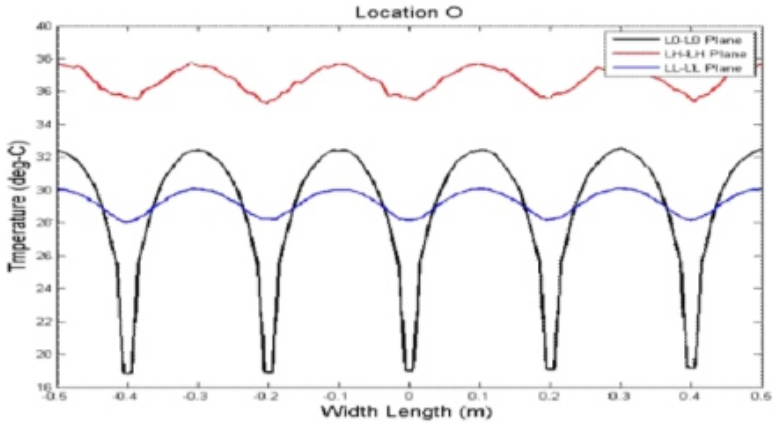

Fig. 7 Distribution of thermal transportation at the cross- sections for the 2-lap crooked pipe layout

c. 6 crooked pipeline through the wall

The groundwater cooling pipe is located in the wall for cooling the wall (water temperature is 19, flow velocity is 0.1 m3/h). When the wall is equipped with 6 crooked cooling pipe (Figure 7-3), the outer wall (Section LH) is exposed to the sun, the temperature rises gradually, the ambient temperature makes the wall temperature higher than 40. However, due to the cooling circuit, the temperature near the pipeline falls to 36; the temperature between the pipelines only rises to 37. The Section L0 shows large temperature difference, the temperature near the pipeline is 19, that between the pipelines rises to 30. As the 6 crooked pipeline is relatively dense, the cooling effect acts on the outer wall section and inner wall section, the maximum temperatures of outer wall section (LH) and cooling pipe distributed section (L0) are 39 and 34, lower than Condition a (2 crooked cooling pipe) by 1-2. The section near the inner wall (Section LL) has decreasing temperature difference, the temperature near the pipeline or between the pipelines is kept at 28-29.

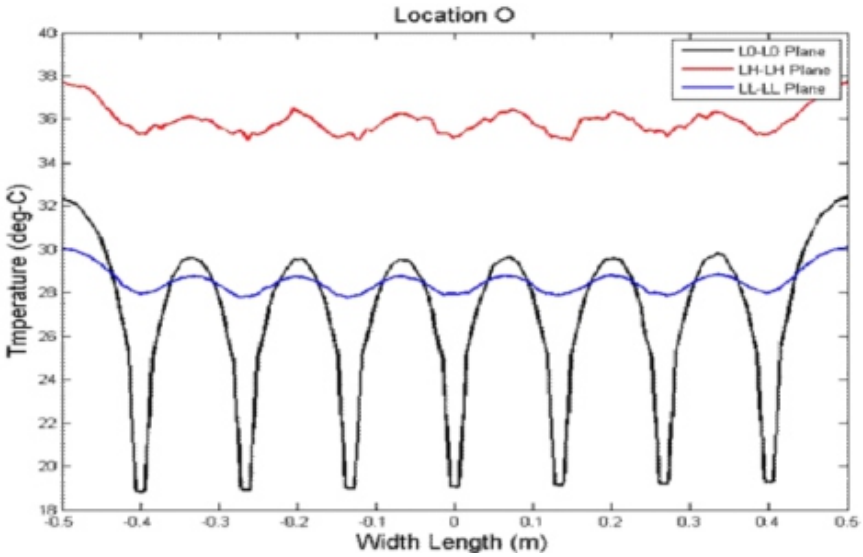

Fig. 8 Distribution of thermal transportation at the crosssections for the 2-lap crooked pipe layout

d. 8 crooked pipeline through the wall

Under conditions 1. 8 crooked cooling pipeline (Figure 9), when the groundwater at 19 flows through the wall; 2 the outer wall condition is affected by sun illumination, its temperature is also higher than 40. The temperature of outer wall (Section LH) is influenced by the cooling circuit, falling to 35 to 36.

The Section L0 shows decreasing temperature difference, the temperature near the pipeline is 19, that between the pipelines rises to about 27. The temperature of the section near the inner wall (Section LL) remains at about 28. Compared with Section L0, the maximum temperature of L0 (temperature between pipelines 27) has been lower than the maximum temperature of Section LL (temperature between pipelines 28). The results show that the heat is not transferred from the outer wall to the interior in this state. The analysis result of this layout also shows that the cooling circuit influences the outer wall, the wall temperature remains at 36. This result will influence the external microclimate, so that the sun illumination will not multiply the thermal effect on the surroundings of wall.

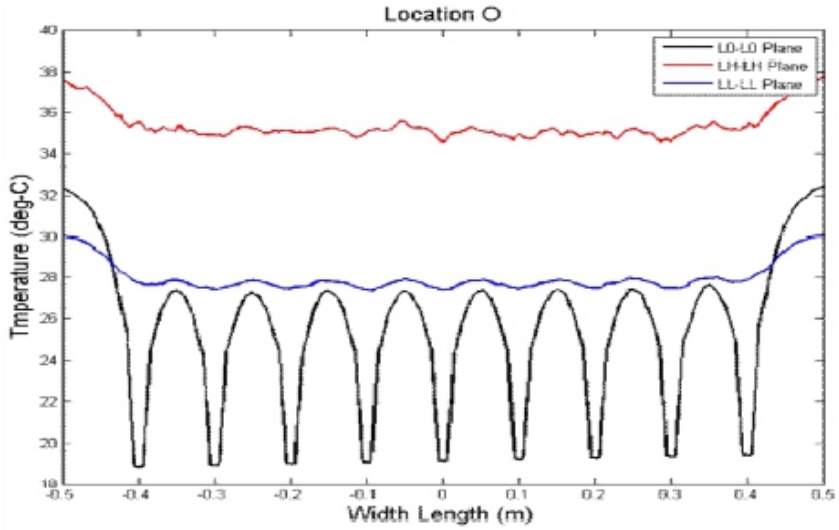

Fig. 9 Distribution of thermal transportation at the cross- sections for the 2-lap crooked pipe layout

CONCLUSIONS

To sum up the experimental analysis and simulation conclusion, this study involves groundwater temperature analysis, construction of underground cooling system, analysis of heat transfer between groundwater and wall, described below:

5.1 Conclusion

1. The groundwater temperature remains stable in various months, the temperature of the water near the surface rises in summer (19-21), but the difference is slight. In terms of weather environment, the daily mean temperature is 29.1 in Taichung in summer, the maximum monthly mean temperature is 35.3 in July, the minimum temperature is 23.8, the maximum instantaneous wind speed is 11.2m/s, and the average wind speed per 10 minutes is 5.2m/s.

2. According to the analysis of quality of groundwater (including alkalinity, iron ion and turbidity which are likely to influence heat exchange condition), the water alkalinity is 124 mg CaCO3/L, the iron ion concentration is lower than instrument detection limit and water quality item nutritive salt, the concentration is in the reasonable range, it is unlikely to scale influencing the temperature exchange.
3. The simulation analysis shows that the maximum temperature of L0 (temperature between pipelines is 27) is lower than the maximum temperature of Section LL (temperature between pipelines is 28), meaning the heat will not be transferred from the outer wall to the interior in this state.
4. The simulation results reveal that the distance between two adjacent pipe sections influences the thermal transfer within the wall. More closely spaced pipe layout will assist in maintaining lower temperature on the inside wall surface.
5. The 6-lap crooked pipe layout is found to be the optimal for the experimental conditions used in this research
6. An appropriate groundwater flow rate is necessary to effectively carry away the heat without wasting the operational energy and associated cost. The simulation results will be valuable references for future implementation of the proposed groundwater- based building cooling system.

ACKNOWLEDGMENTS

This project was funded by Ministry of Science and Technology in Taiwan. The project number is MOST 103-2218-E-167-003-MY2. We acknowledge with thanks all financial support.

REFERENCES

[1] A. S. Zyoud, W. Rühaak, I. Sass , Dynamic numerical modeling of the usage of groundwater for cooling in north east Jordan – A geothermal case study, Renewable Energy, Volume 62, , Pages 63-72. (2014)
[2] F. Ampofo, G. G. Maidment, and J. F. Missenden, Application of groundwater cooling scheme for London Underground network, International Journal of Refrigeration, Volume 34, Issue 8, Pages 2042-2049. (2011)
[3] F. Grant, Characterizing uncertainty in groundwater- source heating and cooling projects in Manitoba, Canada, Energy, Volume 37, Issue 1, Pages 201-206. (2012)
[4] G. Antonio and C. Matteo, Thermal short circuit on groundwater heat pump, Applied Thermal Engineering, Volume 57, Issues 1–2, Pages 107-115. (2013)
[5] Okubo Y., Kim H.-C., Uchida Y., Goto S., Safanda J., Borehole data and climate reconstruction in Korea, Korea– Japan Joint Seminar on Geophysical Techniques for Geothermal Exploration and Subsurface Imaging Proceedings, September 22–26, 2003, pp. 58—63. (2003)
[6] S. Mohammad, H. Al, "Performance characteristics and practical applications of common building thermal insulation materials". Building and Environment, Vol. 40, Issue 3, pp.353-366.(2005)
[7] S.B. Sadineni, S. Madala, R.F. Boehm, "Passive building energy savings: A review of building envelope components". Volume 15, Issue 8, pp. 3617-3631.(2011)
[8] X. S. Heng, and L. Rybach, Development and application of a new, powerful groundwater heat pump system for space heating and cooling. World Geothermal Congress 2005, International Geothermal Association, Antalya, Turkey (2005)

Stagnation Point Flow of Casson Fluid Over Exponentially Stretching Sheet with Variable Thermal Conductivity and Newtonian Heating

1 Kartini Ahmad, 2 Zaharah Wahid, 3 Zahir Hanouf

[1,2,3]Kulliyah of Engineering, International Islamic University Malaysia, Kuala Lumpur, Malaysia

Email: [1]kartini@iium.edu.my, [2]zaharah@iium.edu.my, [3]zahir8@iium.edu.my

ABSTRACT

In this paper, we investigate the effects of variable thermal conductivity and Newtonian heating on the stagnation point flow of Casson fluid over exponentially stretching sheet. The governing partial differential equations which govern the fluid flow are reduced to ordinary differential equations by imposing suitable similarity transformation. The boundary layer equations are solved numerically using a finite-difference scheme for some embedded parameters, such as the Deborah number β, ratio of free stream velocity to stretching rate λ, fluid variable thermal conductivity ε, Prandtl number Pr and Biot number Bi. The velocity and the temperature profiles within the boundary layer region are depicted in the form of graphs.

Keywords: Casson Fluid, Newtonian Heating, Variable Thermal Conductivity.

I. INTRODUCTION

The final output of certain products which have undergone industrial processes very much depend on the rate of stretching and heat transfer. Sometimes, linear stretching is imposed and sometimes, non-linear stretching is essential in order to get the final desired output. Crane [1] was the first to investigate the flow caused by the stretching of a sheet, which was later extended by other researchers, such as Ali [2], who investigated the thermal boundary layer flow by considering nonlinear stretching surface; Kumaran and Ramanaiah [3], who established general quadratic stretching sheet; and, Magyari and Keller [4], who worked on heat and mass transfer on boundary layer flow due to exponentially stretching sheet. Since then, lots of studies have been conducted [5-10].

In general, there are four common heating processes, i.e constant or prescribed wall temperature, constant or prescribed surface heat flux, conjugate conditions, where heat is supplied through a bounding surface or finite thickness, and finite heat capacity and Newtonian heating [11]. A number of studies have been done for the first two cases with scarcely any problems, considering Newtonian heating can be found in the literature. However, lately, this subject has become one of interest. Motivated by the work of Merkin [11], Pop et. al. [12] studied free-convection boundary layer flow along vertical surface embedded in a porous medium with Newtonian heating, Lesnic et al. [13]

investigated steady free convection boundary layer along a semi-infinite, slightly inclined to the horizontal plate embedded in porous medium with the flow generated by Newtonian heating and Salleh et al. [14] worked on forced convection boundary layer flow near the forward stagnation point of an infinite plane wall generated by Newtonian heating. Recently, Mohamed et al. [15] considered stagnation point flow over a stretching surface generated by Newtonian heating, Zeeshan et al. [16] studied the effects of Joule and Newtonian heating on stagnation point flow of Newtonian and non-Newtonian fluids over a stretching cylinder and Lavanya et al. [17] investigated the phenomenon of Newtonian heating under the application of uniform porous medium when heat generation and chemical reactions appear in the energy and volumetric species equations in the flow of a nanofluid. Newtonian heating or so-called conjugate convective flows occurs when heat is supplied to the convective fluid through a bounding surface with a finite heat capacity. This phenomenon can be found in many engineering devices, such as heat exchangers, where the conduction in a solid tube wall is greatly influenced by the convection in the fluid flowing over it.

All the above mentioned works were conducted taking into consideration constant thermal conductivity. However, variable thermal conductivity is more practical. Hence, we would like to extend the work of Nadeem et al. [18] and Bhattacharyya [19], taking into account the effects of variable thermal conductivity and Newtonian heating over exponentially stretching sheet with the absence of radiation and magnetohydrodynamic fields.

II. ANALYSIS

Consider a steady two-dimensional boundary layer flow of Casson fluid near a stagnation point. The x-axis is taken along the stretched sheet and y-axis is normal to it, with the stagnation point at the origin. It is assumed that the flow is to be confined in half plane y> 0 and the sheet is stretched exponentially with velocity U (x) = ae x / L . The sheet is assumed to be heated due to Newtonian heating as proposed by Merkin [11]. The external flow is of the form of U (x) = bex / L and the ambient temperature is T .

Here, a, b are positive constant and L is the characteristic length. Under these assumptions and neglecting the effects of viscous dissipation and heat generation, the boundary layer flow for the problem is given by:

$$\frac{\partial u}{\partial x} + \frac{\partial v}{\partial y} = 0, \quad (1)$$

$$u\frac{\partial u}{\partial x} + v\frac{\partial u}{\partial y} = U\frac{\partial U_\infty}{\partial x} + \upsilon\left(1 + \frac{1}{\beta}\right)\frac{\partial^2 u}{\partial y^2}, \quad (2)$$

$$\rho c_p\left(u\frac{\partial T}{\partial x} + v\frac{\partial T}{\partial y}\right) = \frac{\partial}{\partial y}\left(\kappa^*\frac{\partial T}{\partial y}\right), \quad (3)$$

subject to the boundary conditions:

$$u = U_w, \quad v = 0, \quad \frac{\partial T}{\partial y} = -h_s (T_w - T_\infty) \text{ at } \quad y = 0, \quad (4)$$
$$u \to U_\infty, \quad T \to T_\infty \text{ as } \quad y \to \infty,$$

where u and v are the velocity component along x- and y-axis, respectively, υ is the kinematic viscosity, $\beta = \mu_B \sqrt{2\pi_c} / p_y$ is the Casson fluid parameter, ρ is can be obtained once the values of respectively, are found. $f'(0)$ and $-\theta'(0)$, the density, cp is the specific heat at constant pressure, Tis the fluid temperature in the boundary layer, hs is the heat transfer parameter for the Newtonian heating and κ* is the variable thermal conductivity defined as $\kappa^* = \kappa (1 + \varepsilon\theta)$, where κ is the fluid free stream conductivity and $\varepsilon = \frac{\kappa_w - \kappa}{\kappa}$ is the perturbation/small parameter [20, 21, 22]. In general, $\varepsilon > 0$ is for

fluids, such as water and air, while $\varepsilon < 0$ is for fluids, such as lubrication oil [23].

We look at the solutions of Eqs.(1)-(3) in the following forms [23]:

$$\psi = \sqrt{2\upsilon L a}\, f(\eta) e^{x/2L},$$
$$\eta = y \sqrt{\frac{a}{2\upsilon L}}\, e^{x/2L}, \quad (5)$$
$$\theta(\eta) = \frac{T - T_\infty}{T_\infty},$$

where ψ is the stream function defined in usual notation, i.e $u = \partial\psi / \partial y$ and $v = -\partial\psi / \partial x$. Thus, we have:

$$u = a f'(\eta) e^{x/L},$$
$$v = -\sqrt{\frac{\upsilon a}{2L}} \left[\eta f'(\eta) + f(\eta)\right] e^{x/2L}, \quad (6)$$

where prime denotes differentiation with respect to η. Making use of (5) and (6) into Eqs.(1) - (3), Eq. (1) is automatically satisfied and Eqs. (2) and (3) are reduced to:

$$\left(1 + \frac{1}{\beta}\right) f''' + f f'' - 2(f')^2 + 2\lambda^2 = 0, \quad (7)$$

where prime denotes differentiation with respect to η. Making use of (5) and (6) into Eqs.(1) - (3), Eq. (1) is automatically satisfied and Eqs. (2) and (3) are reduced to:

$$(1 + \varepsilon\theta)\theta'' + \varepsilon(\theta')^2 + Pr\, f\, \theta' = 0, \quad (8)$$

with boundary conditions:

$$f(\eta) = 0, \quad f'(\eta) = 1, \quad \theta'(\eta) = -\text{Bi}\left[1 + \theta(0)\right] \text{ at } \quad \eta = 0,$$
$$f'(\eta) \to \lambda, \quad \theta(\eta) \to 0 \text{ as } \quad \eta \to \infty, \quad (9)$$

where $\lambda = \frac{b}{a}$ is the ratio of free stream velocity parameter to stretching sheet parameter, $Pr = \frac{\mu c_p}{\kappa}$ is the Prandtl number and $Bi = h_s \sqrt{\frac{2\upsilon L}{a}}\, e^{-x/2L}$ is the Biot number. For the momentum and energy equations to have similarity solution, parameter Bi must be a constant and not a function of x. Hence, assume hs = ex / 2 L .From an engineering point of view, there are two physical quantities of interest, i.e skin friction coefficient and local Nusselt number, which can be obtained once the values of respectively, are found.

III. RESULTS AND DISCUSSION

Eqs. (7) and (8) subject to boundary condition (9) have been solved numerically using a finite-difference scheme as described in the book by Cebeci and Bradshaw [24] for some values of λ, β, ε and Bi number.

Fig. 1 depicts the effect of the velocity ratio towards the velocity profile. As λ = b/a, which gives the ratio of the external stream velocity to the sheet velocity, it is found that when λ = 1, no boundary layer is formed and the velocity remains constant (=1) throughout. However, as λ> 1, the velocity starts to increase and the boundary layer thickness decreases as λ> 1. This is due to the increment of the straining motion near the stagnation region, which in turn accelerates the external stream and causes a reduction in the boundary layer thickness. For λ< 1, inverted boundary layer structured is formed. These phenomena are valid for both Newtonian (β = ∞) and Casson fluid flow (β= 1), which validate the boundary condition (9) that we have set. It should be highlighted that the Casson fluid flow is found to have lower velocity than the Newtonian fluid flow when λ> 1, and the opposite situation occurs for λ< 1.

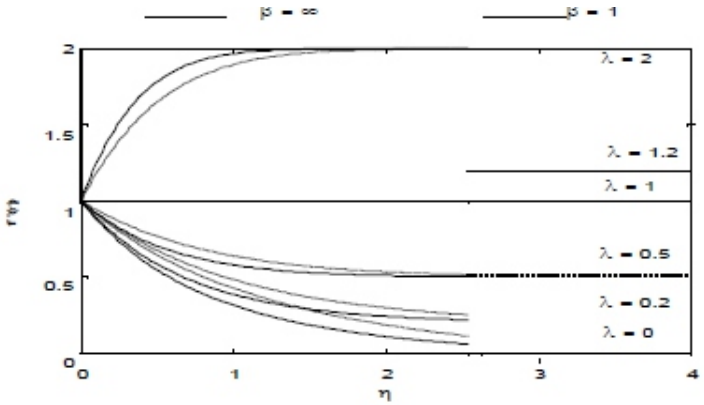

Fig. 1. Velocity profiles for various values of λ for Newtonian flow (β = ∞)and Casson fluid flow (β = 1).

Fig. 2 and 3 represent the effect of the variable thermal conductivity ε in the temperature distribution when λ = 0.2, Pr = 7 and Bi = 0.1 and 0.3, respectively. As ε only exists in the energy equation given by (8), it is expected that ε will have a significant impact on the thermal boundary layer. However, the value

of ε chosen is restricted to some value, especially when ε> 1. This ε can go up to 0.6 when Bi = 0.1 but is limited to 0.2 when Bi = 0.3. At this point (ε = 0.6 and 0.2, respectively), the distribution of the temperature in the boundary layer is reversed, unlike the distribution of the Casson fluid and temperature dissemination when ε< 0.6 and ε< 0.2, respectively. Furthermore, there was a reversed overshoot at the beginning of the thermal boundary layer formation when the flow is dominated by Newtonian fluid (β = ∞). It is also seen that the temperature increases as ε decreases and outstanding results are found to exist when Bi = 0.3 as compared with Bi = 0.1. On top of that, for fixed value of ε, it is observed that the temperature within the boundary layer for Casson fluid flow (β = 1) is slightly lower than the Newtonian flow (β = ∞). As boundary condition (9) is concerned, all the profiles plotted satisfy those conditions.

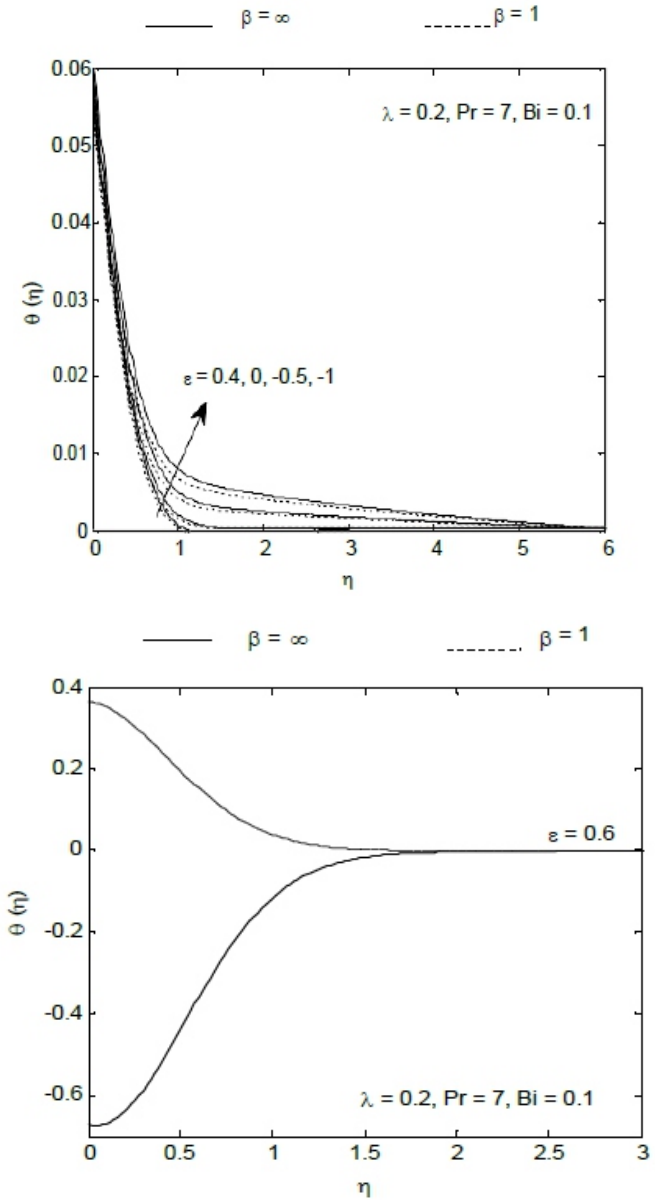

Fig.2.Temperature profiles for various values of ε for Newtonian flow (β = ∞) and Casson fluid flow (β = 1) Whenλ = 0.2, Pr = 7 and Bi = 0.1.

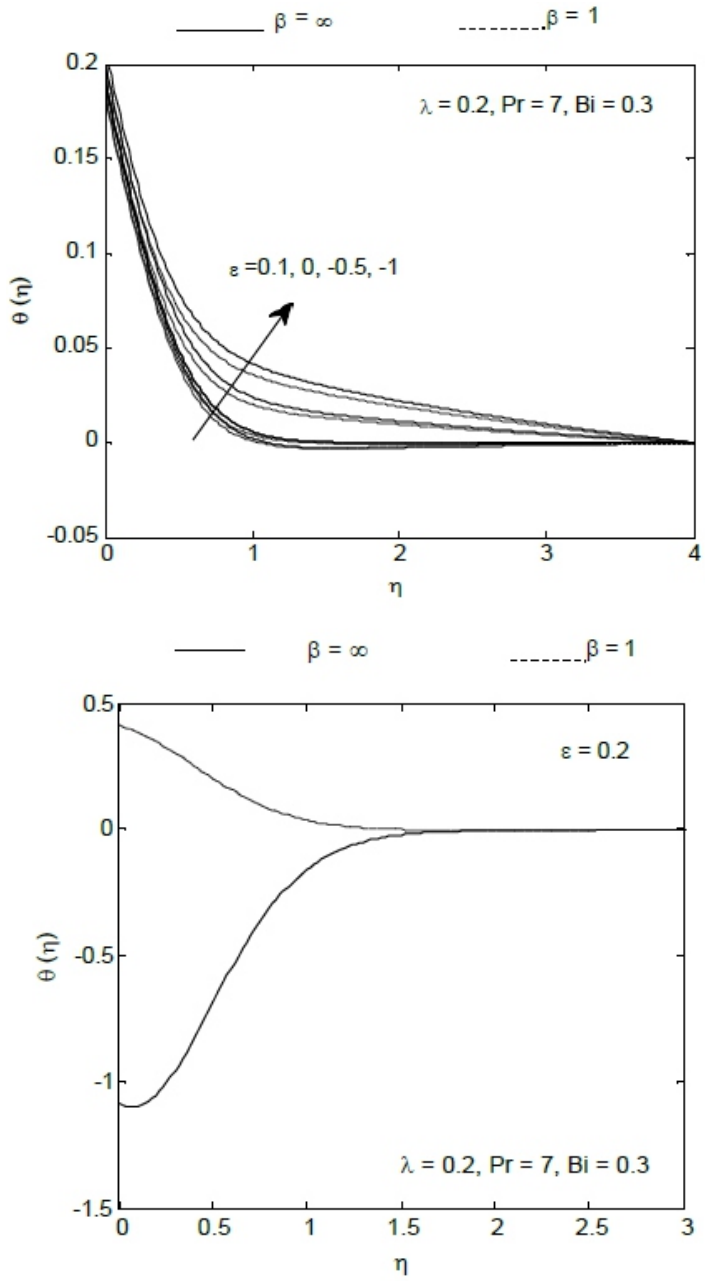

Fig. 3.Temperature profiles for various values of εfor Newtonian flow (β = ∞) and Casson fluid flow (β = 1) when λ = 0.2, Pr = 7 and Bi = 0.3.

CONCLUSIONS

Boundary layer flow of Casson fluid on the stagnation point with the effects of variable thermal conductivity and Newtonian heating over exponentially stretching sheet is investigated. Some of the main results are:

1. The velocity increases for both Newtonian (β = ∞) and Casson fluid flow (β = 1) as λ >0. However, the velocity of Casson fluid flow is slightly higher than Newtonian flow when λ < 1 and an opposite trend is seen for λ > 1. The velocity remains constant throughout the boundary layer when λ = 1.

2. As ε increases, the temperature on the boundary layer is found to decrease. However, the value of ε chosen is limited to certain values, especially when ε > 0. At this point, temperature distribution in the Newtonian and Casson fluid are found to have opposite features.
3. Casson fluid flow is found to decrease the temperature as compared with Newtonian fluid flow within the boundary layer.

ACKNOWLEDGMENT

The authors are grateful for the financial support received in the form of grant by Ministry of Higher Education Malaysia (FRGS 15-228-0469).

REFERENCES

1. *L. J. Crane, "Flow past a stretching sheet," Z. Angew. Math. Phys., vol. 21, pp. 645-647, 1970.*
2. *M. E. Ali, "On thermal boundary layer on a power law stretched surface with suction or injection," Int. J. Heat Fluid Flow, vol. 16, pp. 280-290, 1995.*
3. *V. Kumaran and G. Ramanaiah, "A note on the flow over a stretching sheet," Acta Mech., vol. 116, pp. 229-233, 1996.*
4. *E. Magyari and B. Keller, "Heat and mass transfer in the boundary layers on an exponentially stretching continuous surface," J. Physics, vol. 32, pp. 577-585, 2000.*
5. *S. A. Kechil, "Flow and diffusion of chemically reactive species over a nonlinearly stretching sheet immersed in a porous medium," Journal of Porous Medium, vol. 12, no. 11, pp. 1053-1063, 2009.*
6. *J. Zhu, L. C. Zheng and X. H. Chen, "Similarity solutions of the MHD stagnation-point flow over a power-law stretching sheet," Applied Mechanics and Materials, vols. 52-54, pp. 1895-1900, 2011.*
7. *M. I. Anwar, A. R. Kasim, M. Z. Salleh, S. Shafie, "Radiation effect on MHD stagnation-point flow of a nanofluid over nonlinear stretching sheet with convective boundary condition," Heat Transfer Research, DOI: 10.1615/HeatTransRes.2016007840, 2013.*
8. *S. W. Wong, A. O. Awang and A. Ishak, "Stagnation point flow over an exponentially shrinking/stretching sheet," A Journal of Physical Sciences, vol. 66, no. 12, pp. 705-711, 2014.*
9. *A. Rahmen, G. Farooq, I. Ahmed and M. Naseer, "Boundary layer stagnation-point flow of second grade fluid over an exponentially stretching sheet," American Journal of Applied Mathematics and Statistics, vol. 3, no. 6, pp. 211-219, 2015.*
10. *K. Ahmad, Z. Hanouf and A. Ishak, "Mixed convection Jeffrey fluid flow over an exponentially stretching sheet with magnetohydrodynamic effect," AIP Advances, DOI: 10.1063/1.4945401, 2016.*
11. *J. H. Merkin, "Natural-convection boundary layer flow on a vertical surface with Newtonian heating," International Journal of Heat and Fluid Flow, vol. 15, no. 5, pp. 392-398, 1994.*
12. *I. Pop, D. Lesnic and D. B. Ingham, "Asymptotic solutions for free convection boundary-layer flow a long a vertical surface in a porous medium with Newtonian heating," Hybrid Methods in Engineering, vol. 2, no. 1, doi: 10.1615/HybMethEng.v2.i1.30, 2000.*
13. *D. Lesnic, D. B. Ingham and I. Pop, "Free convection boundary layer flow above a nearly horizontal surface in a porous medium with Newtonian heating," Heat and Mass Transfer, vol. 40, no. 9, pp. 665-672, 2004.*
14. *M. Z. Salleh, R. Nazar and I. Pop, "Forced convection boundary layer flow at a forward stagnation point with Newtonian heating," Chemical Engineering Communications, vol. 196, no. 9, pp. 987-996, 2009.*
15. *M. K. A. Mohamed, M. Z. Salleh, R. Nazar and A. Ishak, "Stagnation point flow over a stretching sheet with Newtonian heating," SainsMalaysiana, vol. 41, no. 11, pp. 1467-1473, 2012.*
16. *A. Zeeshan, R. Ellahi, S. Abbasbandy and S. Rashidi "Joules and Newtonian heating effects on stagnation point flow over a stretching surface by means of generic algorithm and Nelder-Mead method," International Journal of Numerical Methods for Heat and Fluid Flow, vol. 25, no. 3, pp. 665-684, 2015.*
17. *M. Lavanya, M. S. Babu and G. V. Ramaniah, "Heat transfer of nanofluid past an exponentially permeable stretching sheet with heat generation and Newtonian heating in a porous medium," International Journal of Innovative Research and Development, vol. 5, no. 1, pp. 318-329, 2016.*
18. *S. Nadeem, R. U. Haq and C. Lee, "MHD flow of a Casson fluid over and exponentially shrinking sheet," Scientia Iranica, vol. 19, no. 6, pp. 1550-1553, 2012.*

19. K. Bhattacharyya, "MHD stagnation-point flow of Casson fluid and heat transfer over a stretching sheet with thermal radiation," Journal of Thermodynamics, vol. 2013, article ID 169674, 9 pages, 2013.
20. M. Arunachalam and N. R. Rajappa, "Forced convection in liquid metals with variable thermal conductivity and capacity," ActaMechanica, vol. 31, no. 1-2, pp. 25-31, 1978.
21. T. C. Chiam, "Heat transfer in a fluid with variable thermal conductivity over stretching sheet," ActaMechanica, vol. 129, no. 1-2, pp. 63-72, 1998.
22. P.R. Sharma and G. Singh, "Effects of variable thermal conductivity and heat source/sink on MHD flow near a stagnation point on a linearly stretching sheet," Journal of Applied Fluid Mechanics, vol. 2, no. 1, pp. 13-21, 2009.
23. S. Jain and R. Choudhary, "Effects of MHD on boundary layer flow in porous medium due to exponentially shrinking sheet with slip," in Procedia Engineering, 2015, vol. 127, pp. 1203-1210.
24. T. Cebeci and P. Bradshaw, Physical and Computational Aspects of Convective Heat Transfer, New York: Springer, 1988.

Performance of Multiple Tuned Liquid Column Dampers in Vibration Control of Structures under Real Earthquake Excitation

[1] Rama Debbarma, [2] Debasis Panda, [3] Arka Mitra

[1]PhD, Associate Professor,

[2,3] M.Tech Scholar, Department of Civil Engineering, National Institute of Technology Agartala, India-799046

E-mail: [1] ramadebbarma@gmail.com, [2]debasispanda777@gmail.com, [3]arkamitra080@gmail.com

ABSTRACT

The effectiveness of Multiple Tuned Liquid Column Dampers (MTLCD) in suppressing structural vibrations considering different real earthquake time history data is investigated using a numerical method to deal with the nonlinearity of the governing equations in this paper. It was found that increasing the number of TLCDs can enhance the efficiency of the MTLCD. The study also shows that effectiveness of the MTLCD to reduce structural displacement and acceleration is highly dependent on the nature of the earthquake excitation. The results also confirm that although the performance of the proposed TCLD vary with the nature of the earthquakes, but overall it performs exceptionally well for all earthquakes, by standing out the maximum structural displacements and also rapid response decay.

Keywords - Real earthquake time history, vibration control, multiple tuned liquid column dampers, tuned liquid column dampers.

I. INTRODUCTION

Tuned Liquid Column Damper (TLCD), as a passive vibration control device can suppress the input energy by the combined action of the movement of the mass in the U-shaped container, the restoring force on the liquid due to gravity and the damping due to liquid movement through the orifices. Because there are a number of inherent advantages in this device including its lower implementation cost, easier handling and lower maintenance cost, and like other passive devices, they do not usually interfere with vertical and horizontal load paths, has become more popular in this days. Sakai et al (1989) proposed the nonlinear mathematical expression of the TLCD. Later many authors used the linearized equation of motion to investigate the effectiveness of the TLCD to suppress the structural vibration using a frequency domain analysis. Later Gao et al. (1997) carried out a numerical study to find out the optimum parameters of a TLCD to minimize the peak structural response under harmonic excitations in a wide range of frequency for flexible structures In recent years many experimental and theoretical studies have been carried out on the evaluation of TLCD performance in suppressing the structural vibrations. However most of them have investigated the performance of TLCD under sinusoidal loadings, wind excitations, and relatively few studies has been carried out on the seismic performance of TLCDs (Won et al.,1996; Debbarma et al., 2010; Chakraborty et al. 2012). In this paper the performance of Multiple Tuned Liquid Column Dampers (MTLCD) in suppressing structural vibrations considering different

real earthquake time history data is investigated using a numerical time domain method (The Newmark-beta linear acceleration method) to deal with the nonlinearity of the governing equations in this paper. A parametric numerical study involving the effects of the parameters like mass ratio, frequency tuning ratio, length ratio, and blocking ratio is carried out for different seismic time history data, using a to deal with the nonlinearity of the governing equations. It was found that increasing the number of TLCDs can enhance the efficiency of the MTLCD. The study also shows that effectiveness of the MTLCD to reduce structural displacement and acceleration is highly dependent on the nature of the earthquake excitation. The results also confirm that although the performance of the proposed TCLD vary with the nature of the earthquakes, but overall it performs exceptionally well for all earthquakes, by standing out the maximum structural displacements and also rapid response decay.

II. THE EQUATION OF MOTION OF STRUCTURE AND MTLCD SYSTEM

A TLCD is a U-shaped liquid column tube attached to a primary structure. A building is modeled as a SDOF structure and n no of TLCDs are mounted on top of the primary structure as shown in Fig. 1.

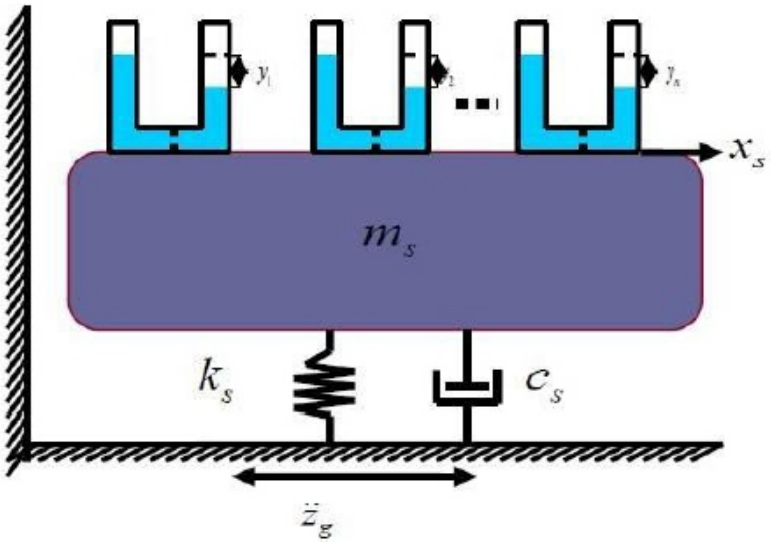

Fig.1: Simplified MTLCD-structure system

Assumed the liquid density(generally water) to be ρ, and the cross section area, horizontal length, vertical height of liquid of the ith TLCD of the MTLCD are represented by Ai, Bi, hi and. The total length of the liquid column of the ith TLCD is, Li = (Bi+2hi). The total mass of the damper, $m_d = \sum_{i-1} \rho A L$, ignoring the mass of the liquid container, which can be included within the mass of the primary structure.

2.1 The equation of motion of MTLCD:

Due to the earthquake motion the structure-MTLCD system is subjected to base acceleration 'z'b . If the relative horizontal displacement of SDOF system and the liquid surface displacement is represented by

x and y, the equation of motion of liquid column can be expressed as

$$\rho A_i L_i \ddot{y}_i + \frac{1}{2}\rho A_i \xi_i |\dot{y}_i| \dot{y}_i + 2\rho g A_i y_i = -\rho A_i B_i \{\ddot{x} + \ddot{z}_b\}, i = 1 \ldots . n \quad (1)$$

Normalizing the above equation

$$\ddot{y}_i + \frac{\xi_i}{2L_i} |\dot{y}_i| \dot{y}_i + \omega_{di}^2 y_i + p_i \ddot{x} = -\ddot{z}_b \quad (2)$$

Where $p_i = \frac{B_i}{L_i}$ is the length ratio of ith TLCD (Length ratio is the length of the horizontal portion of TLCD to its total length), $\omega_{di} = \sqrt{\frac{2g}{L_i}}$ is the frequency of the liquid motion and ωs is the frequency of the primary structure and the co- efficient of head loss, ξ is determined using

$$\xi = \left(-0.6\varphi + 2.1\varphi^{0.1}\right)^{1.6} (1-\varphi)^{-2} \quad (3)$$

by Wu et al (2005).

Where φ is the blocking ratio.

2.2 The equation of motion of structure with MTLCD:

The equation of motion of primary structure with TLCD can be written as

$$(m_s + m_d)\ddot{x} + c_s\dot{x} + k_s x = -(m_s + m_d)\ddot{z}_b - \rho A_i p_i L_i y_i \quad (4)$$

Where, m_s , k_s , c_s are the mass, stiffness and damping of the primary structure. Simplifying the above equation

$$(1+\mu)\ddot{x} + 2\xi_s \omega_s \dot{x} + \omega_s^2 x + \mu_i p_i y_i = -(1+\mu)\ddot{z}_b \quad (5)$$

Where, $\mu_i = \frac{\rho A_i L_i}{m_s}$ mass ratio of ith TLCD, $c_s = 2\xi_s \omega_s m_s$ and $\omega_s = \sqrt{\frac{k_s}{m_s}}$.

By combining Eqns. (2) and (5), the equation of motion of structure-MTLCD system in matrix form can be written as

$$M\ddot{Y} + C\dot{Y} + KY = -M\ddot{z}_b \quad (6)$$

Where M, C, K represents the mass, damping and stiffness matrix of the combined system respectively Y represent the relative displacement vector. They have the following forms:

$$M = \begin{bmatrix} 1+\mu & \mu_1 p_1 & \mu_2 p_2 & \cdots & \cdots & \mu_n p_n \\ \mu_1 p_1 & \mu_1 & 0 & \cdots & \cdots & 0 \\ \mu_2 p_2 & 0 & \mu_2 & \cdots & \cdots & 0 \\ \vdots & \vdots & \vdots & \ddots & \vdots & \vdots \\ \vdots & \vdots & \vdots & \vdots & \ddots & \vdots \\ \mu_n p_n & 0 & 0 & \cdots & \cdots & \mu_1 \end{bmatrix} \quad (7)$$

$$K = \omega_s^2 \begin{bmatrix} 1 & 0 & 0 & \cdots & \cdots & 0 \\ 0 & \mu_1\gamma_1^2 & 0 & \cdots & \cdots & 0 \\ 0 & 0 & \mu_2\gamma_2^2 & \cdots & \cdots & 0 \\ \vdots & \vdots & \vdots & \ddots & \vdots & \vdots \\ \vdots & \vdots & \vdots & \vdots & \ddots & \vdots \\ 0 & 0 & 0 & \cdots & \cdots & \mu\lambda_{nn}^2 \end{bmatrix} \quad (8)$$

$$C = \begin{bmatrix} 2\xi s\omega s & 0 & 0 & \cdots & \cdots & 0 \\ 0 & \frac{\mu_1}{2L_1} y_1 \dot{y} & 0 & \cdots & \cdots & 0 \\ 0 & 0 & \frac{\mu^2}{2L_2} y_2 \dot{y} & \cdots & \cdots & 0 \\ \vdots & \vdots & \vdots & \ddots & \vdots & \vdots \\ \vdots & \vdots & \vdots & \vdots & \ddots & \vdots \\ 0 & 0 & 0 & \cdots & \cdots & \frac{\mu}{2Ln} y_n \dot{y}_n \end{bmatrix} \quad (9)$$

$$\bar{r} = \begin{bmatrix} 1 & 0 & 0 & 0 & \cdots & 0 \end{bmatrix}^T \quad (10)$$

$$Y = \begin{bmatrix} x & y_1 & y_2 & \cdots & \cdots & y_n \end{bmatrix}^T \quad (11)$$

III. NUMERICAL STUDY

A building is modeled as a SDOF structure and a MTLCD mounted on top of the primary structure as shown in Fig. 1, used for the analysis. The properties of primary structure are ms=3.0×10^5 kg, ks=8.2247×106 N/m and damping ratio of structures, $\xi s = 2\%$ .The structure has a natural frequency f1 =0.8333 Hz. For the sake of simplicity and convenience some assumptions on a MTLCD with n TLCDs are made:

(i) A MTLCD consists of n number of TLCDs and n is an odd number (1.3, 5…..n).

(ii) The tuning ratio of a MTLCD is decided by the frequency ratio of the central TLCD

$$\gamma = \frac{(\gamma_{n-1} + \gamma_o)}{2}, \quad \gamma_o \text{ taken as 1.}$$

(iii) The mass ratio and coefficient of head loss of each TLCD are same $\mu_i = \frac{\mu}{n}$, μ taken as 5% and, ξ taken using equation 3.

(iv) The frequency range of MTLCD, $\Delta\gamma$, defined as $\Delta\gamma = \gamma n - \gamma 1$

(v) The spacing between TLCD natural frequencies $\delta\gamma$ is constant $\delta\gamma = \gamma i+1 - \gamma i$ $\delta\gamma$, taken as 0.05.

To know the impact of seismic excitations on the performance of MTLCD, some past earthquake ground motion records are selected for the analysis. The structure is analyzed without MTLCD and with

a MTLCD attached to the top of the structure. The structure without and with one, three and five number of TLCD is subjected to previously selected past earthquake data of Park field earthquake (1966), EL-Centro earthquake (1940), Mammoth lake earthquake (1980), and Coalinga earthquake (1983).

The variation of displacements of structures with time considering time history data of previously selected earthquakes using three and five TLCDs and without damper have been shown in Figs. 2 and the Values of maximum displacement of structure without and with one, three, and five TLCDs and corresponding effectiveness of MTLCD have been shown Table-1.

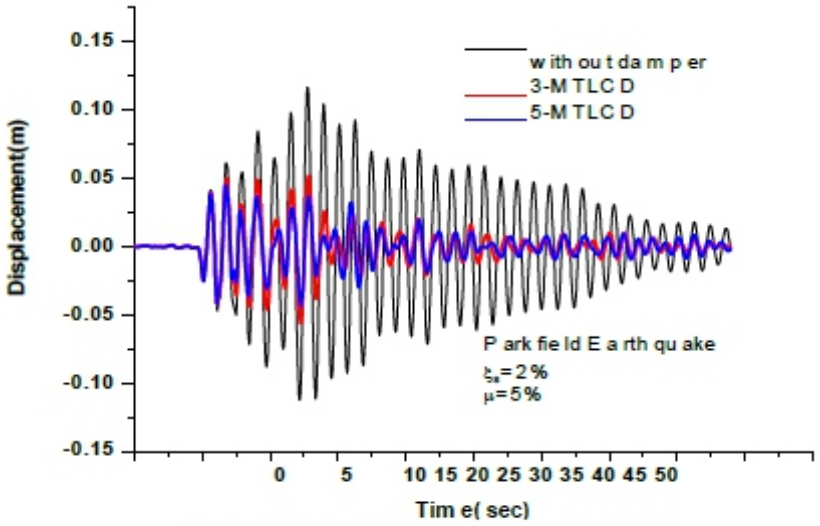

(a) Parkfield earthquake (1966).

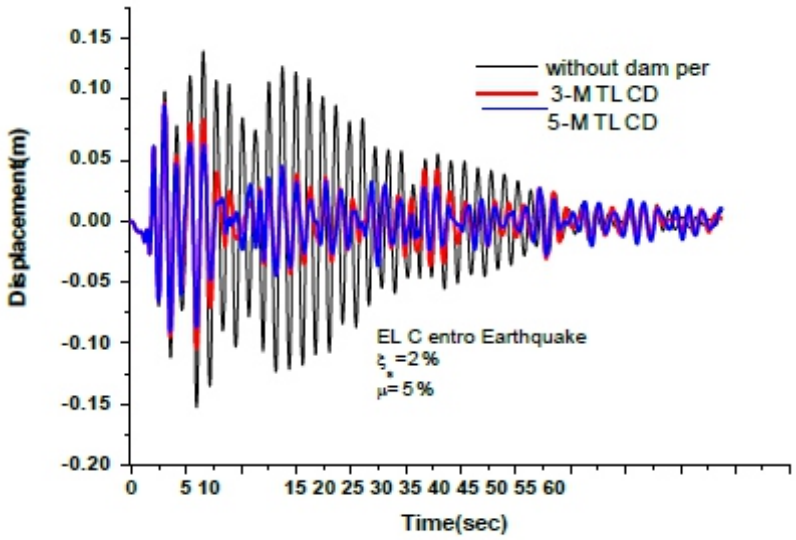

(b) EL-Centro earthquake (1940).

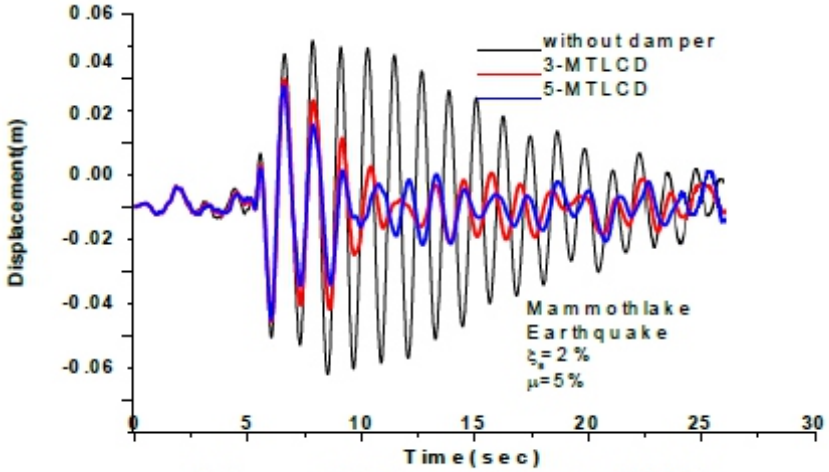

(c) Mammoth lake earthquake (1980).

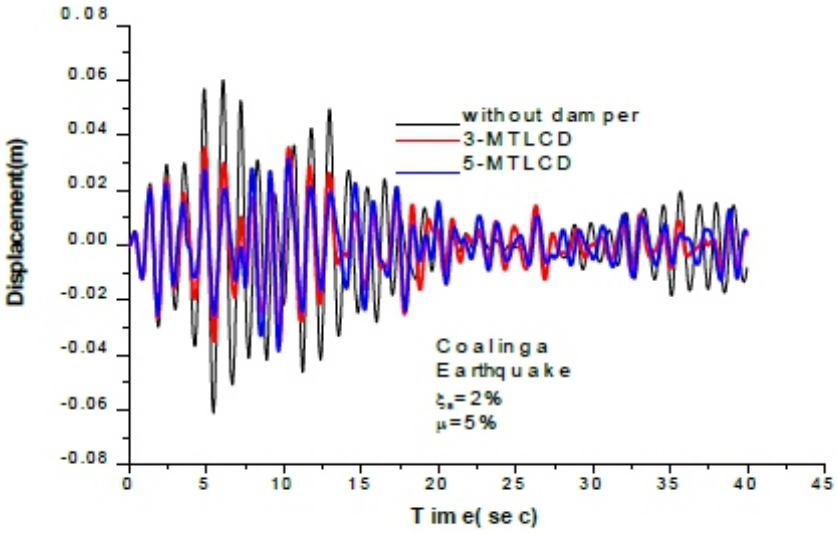

(d) Coalinga earthquake,(1983).

Fig. 2: Variation of displacement of structures considering real time history data of (a) Parkfield earthquake (1966), (b) EL- Centro earthquake (1940),(c)Mammoth lake earthquake (1980),(d) Coalinga earthquake,(1983), for total Mass ratio = 5%, Damping ratio of structures=2% and, Length ratio=0.8.

The results show that the effectiveness of the MTLCD to reduce the structural displacement is increasing with the increase of number of TLCDs i.e. for same mass ratio and for Parkfield, EL-Centro earthquake, Coalinga, and Mammoth lake earthquake data, and for single TLCD the peak displacement reductions are 52.05%, 31.63%, 40.26%, and 24.14% respectively while for same mass ratio and for five TLCDs the peak displacement reductions are 55.48%, 34.58%, 43.04% and 27.39% respectively.

The variation of acceleration of structures with time using three and five TLCDs and without damper have been shown in Figs. 3 and the Values of maximum acceleration of structure without and with one,

three, and five TLCDs and corresponding effectiveness of MTLCD considering time history data of Parkfield earthquake (1966), EL-Centro earthquake (1940), Mammoth lake earthquake (1980), and Coalinga earthquake (1983), have been shown in Table-2.

Table-1: Values of maximum displacement of structure without and with MTLCD and corresponding effectiveness of MTLCD taking structural damping=2%, total mass ratio=5%, blocking ratio=0.1 and length ratio=0.8

Earthquakes	Maximum displacement(m)				% Reduction		
	No control	With TLCD			With TLCD		
		No of TLCDs			No of TLCDs		
		1	3	5	1	3	5
Parkfield	0.1168	0.056	0.055	0.052	52.05%	52.91%	55.48%
El -centro N-S	0.1524	0.1042	0.102	0.0997	31.63%	33.07%	34.58%
Mammoth Lake	0.0522	0.0396	0.039	0.0379	24.14%	25.29%	27.39%
Coalinga	0.0611	0.0365	0.035	0.0348	40.26%	42.72%	43.04%

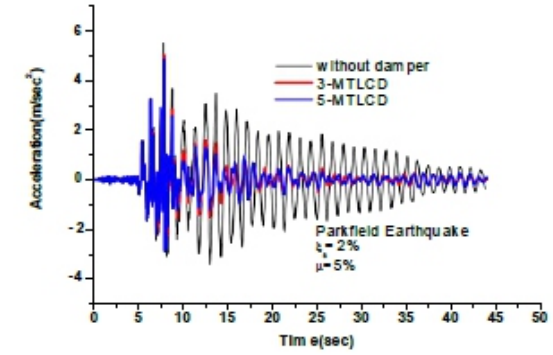

(a) Parkfield earthquake (1966).

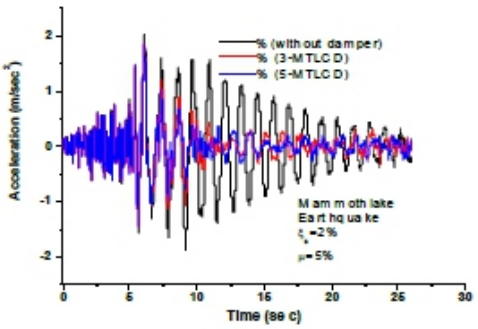

(c) Mammoth lake earthquake (1980).

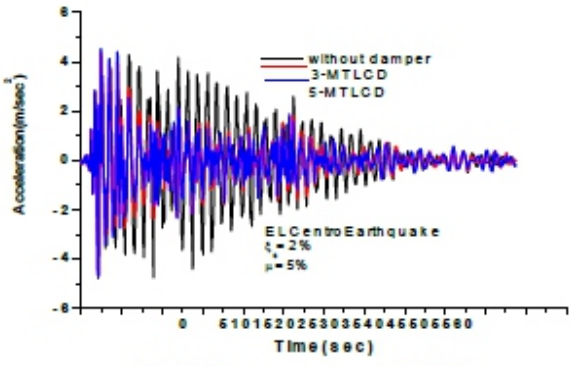

(b) El Centro earthquake (1940).

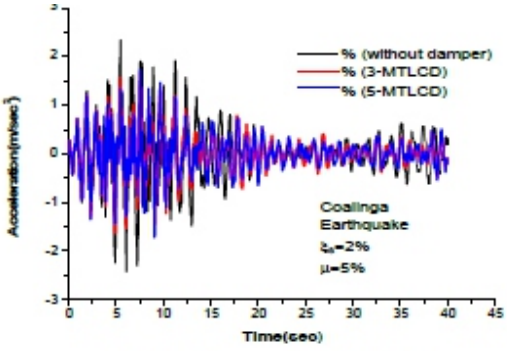

(d) Coalinga earthquake (1983).

Fig. 3: Variation of acceleration of structures considering real time history data of (a) Parkfield earthquake (1966), (b) EL-Centro earthquake (1940), (c) Mammoth lake earthquake (1980), (d) Coalinga earthquake (1983), for total mass ratio=5%, Damping ratio of structures=2%, Length ratio=0.8.

Table-2: Values of maximum acceleration of structure without and with MTLCD and corresponding effectiveness of MTLCD taking structural damping=2%, total mass ratio=5%, blocking ratio=0.1 and length ratio=0.8

Earthquakes	Maximum structural acceleration(m/sec^2)				% Reduction		
	No control	With TLCD			With TLCD		
		No of TLCDs			No of TLCDs		
		1	3	5	1	3	5
Parkfield	5.5168	5.014	4.5848	4.4903	9.11%	16.89%	18.61%
El -centro N-S	4.7706	4.6369	4.5783	4.337	2.80%	4.03%	9.09%
Mammoth Lake	2.0252	1.8522	1.67127	1.5611	8.54%	17.48%	22.92%
colingo	2.4205	1.6586	1.5668	1.4916	31.48%	35.27%	38.38%

From Fig. 2 and Table-2 one can see that peak structural acceleration reduction capacity of MTLCD is increasing with increase of the number of TLCDs. From Fig. 2 and Table-2 it also evident that that peak structural acceleration reduction capacity of MTLCD is not that much significant, this problem is important for acceleration sensitive component, such as non structural components, although this observation needs more extensive analysis for confirmation. The results also confirm that the effectiveness of the MTLCD to reduce structural response is highly dependent upon the nature of the excitations but overall it performs exceptionally well for all earthquakes, by standing out the maximum structural displacements and also rapid response decay.

CONCLUSIONS

A parametric study was carried out to know the effectiveness of MTLCD in suppressing structural vibration due to the seismic excitations. The result of the study shows that with the proper design parameters MTLCD is efficient to reduce peak structural displacement due to the seismic excitations while the peak acceleration reduction capacity is comparatively less, but overall structural displacement and acceleration capacity is very efficient and although the structural displacement and acceleration reduction capacity of TLCD highly depends on the nature of the excitation but overall it performs exceptionally well for all earthquakes, by standing out the maximum structural displacements and also rapid response decay. The study also shows that an optimized MTLCD can be more effective than an optimized single TLCD, the effectiveness of a MTLCD increases as the number of TLCDs comprising a MTLCD increases.

REFERENCES

[1] Sakai F, Takaeda S. Tamaki T. [1989] "Tuned liquid column damper – new type device for suppression of building vibration," Proceedings of the International Conference on High-rise Buildings, Nanjing, China, pp. 926-931.

[2] Won, A.Y.J., Pires, J.A., Haroun, M.A. [1996] "Stochastic seismic performance evaluation of tuned liquid column dampers," Earthquake Engineering & Structural Dynamics 25, 1259–1274.

[3] Gao H, Kwok KCS, Samali B. [1997] "Optimization of tuned liquid column dampers", Engineering structures 19(6), 476- 86.

[4] Wu, J.-C., Shih, M-H., Lin, Y-Y, Shen, Y-C. [2005] "Design guidelines for tuned liquid column damper for structures responding to wind," Engineering Structures 27, 1893-1905.

[5] Debbarma, R., Chakraborty, S., Ghosh, S. [2010] "Unconditional reliability based design of tuned liquid column dampers under stochastic earthquake load considering system parameters uncertainties," Journal of Earthquake Engineering, 14,970-988.

[6] Chakraborty, S., Debbarma, R., Marano. [2012] "Performance of tuned liquid column dampers considering maximum liquid motion in seismic vibration control," Journal of sound and vibration 331, 1519-1531.

Response Mitigation of Structures using Liquid Column Vibration Absorber Considering Real Earthquake Ground Motions

[1] Debasis Panda, [2] Rama Debbarma, [3] Arka Mitra

[1,3]M.Tech Scholar,

[2]PhD, Associate Professor,

Department of Civil Engineering, National Institute of Technology Agartala, India-799046

E-mail: [1]debasispanda777@gmail.com, [2] ramadebbarma@gmail.com, [3] arkamitra080@gmail.com

A B S T R A C T

- The performance of Liquid Column Absorber (LCVA) to mitigate structural vibrations considering different real earthquake time history data is investigated in this paper. To evaluate the significance of the parameters like mass ratio, frequency tuning ratio, length ratio, and area ratio, on the effectiveness of the LCVA for different earthquakes, a similar parametric analysis is performed using a time domain method. The result of the study shows that LCVA is very much effective in reducing the structural response to seismic excitations and the parameters play significant role in the performance of LCVA and some of them are also sensitive to the nature of the excitation.

Keywords - Real earthquake time history, liquid column vibration absorber, vibration control, parametric study.

I. INTRODUCTION

Liquid dampers become more popular in recent days to reduce the seismic responses of structures, due to their low implementation cost, easier handling and low maintenance cost, and like other passive devices, they do not usually interfere with vertical and horizontal load paths. One of these devices, the Tuned Liquid Column Damper (TLCD), suppress the input energy by the combined action of the movement of the mass in the U-shaped container, the restoring force on the liquid due to gravity and the damping due to liquid movement through the orifices. Tuned Liquid Column Damper (TLCD), LCVA is one type of TLCD whose vertical cross section area is different from its horizontal cross sectional area. Sakai et al (1989) proposed the nonlinear mathematical expression of the TLCD. Watkins (1991) tested a different TLCD, the liquid column vibration absorber (LCVA). In recent years many experimental and theoretical studies have been carried out on the evaluation of LCVA performance in suppressing the structural vibrations. However most of them have investigated the performance of LCVA under sinusoidal loadings, wind excitations, and relatively few studies has been carried out on the seismic performance of LCVAs (Chang and Hsu 1998; Chakraborty et al. 2011).

In this paper the performance of Tuned Liquid Column Damper (LCVA) to control the earthquake induced structural vibrations is investigated using different past earthquake data. A similar parametric

numerical analysis, involving the effects of the parameters like mass ratio, frequency tuning ratio, length ratio, and blocking ratio is carried out for different seismic time history data, using a time domain method (The Newmark-beta linear acceleration method) to deal with the nonlinearity of the governing equations, the variations of the different parameters are noted for different natures of the excitation. It is shown that the effectiveness of LCVA to reduce structural displacement and acceleration are very much dependent upon the nature of the earthquakes but overall it performs exceptionally well for all earthquakes. Although the parameters like mass ratio, frequency tuning ratio, length ratio, area ratio play significant role in the performance of LCVA and some of them are also sensitive to the nature of the excitation, few general conclusions are made in which the LCVA is more effective.

II. THE EQUATION OF MOTION OF STRUCTURE AND LCVA SYSTEM

A LCVA is a U-shaped liquid column tube whose vertical cross section area is different from its horizontal cross sectional area is attached to the top of a primary structure. A building is modeled as a SDOF structure and a LCVA is mounted on top of the primary structure as shown in Fig. 1.

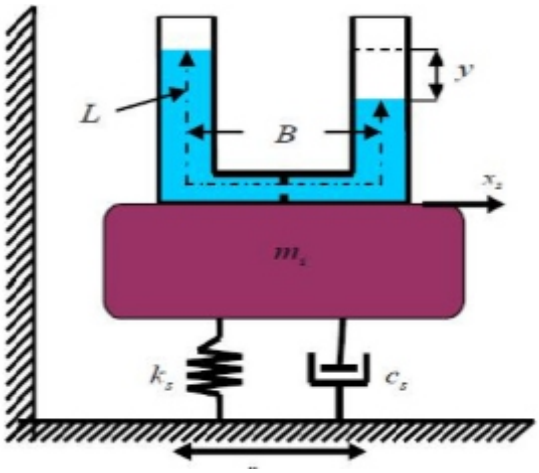

Fig.1: Simplified LCVA-structure system

The horizontal and vertical cross section area, horizontal length, vertical height of liquid and the liquid mass density (generally water) are represented by Ah, Av, B, h and ρ respectively. The total length of the liquid column is, L = (B+2h). The mass of the damper, m d = (ρ A h B + 2 ρ A v h) , ignoring the mass of the liquid container, which can be included within the mass of the primary structure.

2.1 The equation of motion of LCVA:

Due to the earthquake motion the structure-LCVA system is subjected to base acceleration 'z' b . If the relative horizontal displacement of SDOF system and the liquid surface displacement is represented by x be

$$\rho A_h L_{ee} \ddot{y} + \frac{1}{2}\rho A_h \xi |\dot{y}| \dot{y} + 2\rho g A_h y = -\rho A_h B(\ddot{x} + \ddot{z}_b) \quad (1)$$

Normalizing the above equation by liquid mass in the container, ρAh Lee

$$\ddot{y} + \frac{\xi |\dot{y}| \dot{y}}{2L_{ee}} + \frac{2g}{L_{ee}} y + \rho \frac{L}{L_{ee}} \ddot{x} = -\rho \frac{L}{L_{ee}} \ddot{z}_b \quad (2)$$

Where $p = \frac{B}{L}$ is the length ratio. (Length ratio is the length of the horizontal portion of LCVA to its total length). Tuning ratio $\gamma = \frac{\omega_d}{\omega_s}$, where $\omega_d = \sqrt{\frac{2g}{L_{ee}}}$ is the frequency of the damper where $L_{ee} = L\{1 + p(r-1)\}$ and ω_s is the frequency of the primary structure and area ratio $r = \frac{A_v}{A_h}$

The co-efficient of head loss, ξ is determined using equation (3) (By Wu et al. 2005).

$$\xi = \left(-0.6\varphi + 2.1\varphi^{0.1}\right)^{1.6} \left(1 - \varphi\right)^{-2} \quad (3)$$

Where φ is the blocking ratio.

2.2 The equation of motion of structure with LCVA:

The equation of motion of primary structure with LCVA can be written as

$$(m_s + m_d)\ddot{x} + c_s\dot{x} + k_s x = -(m_s + m_d)\ddot{z}_b + r\rho A_h B\ddot{y} \quad (4)$$

Where, m_s, k_s, c_s are the mass, stiffness and damping of the primary structure.

Simplifying the above equation

$$(1+\mu)\ddot{x} + 2\xi_s\omega_s\dot{x} + \omega_s^2 x + \frac{\mu p L}{L_{em}}\ddot{y} = -(1+\mu)\ddot{z}_b \quad (5)$$

Where, $\mu = \frac{(\rho A_h B + 2\rho A_v h)}{m}$ (mass ratio), $c_s = 2\xi_s\omega_s m_s$ and $L_{em} = \left(\frac{B}{r} + 2h\right)$.

From Eqns. (2) and (5)

$$\begin{bmatrix} (1+\mu) & \frac{\mu p L}{L_{em}} \\ \frac{pL}{L_{ee}} & 1 \end{bmatrix} \begin{Bmatrix} \ddot{x} \\ \ddot{y} \end{Bmatrix} + \begin{bmatrix} 2\xi_s\omega_s & 0 \\ 0 & \frac{\xi|\dot{y}|}{2L_{ee}} \end{bmatrix} \begin{Bmatrix} \dot{x} \\ \dot{y} \end{Bmatrix} + \begin{bmatrix} \omega_s^2 & 0 \\ 0 & \frac{2g}{L_{ee}} \end{bmatrix} \begin{Bmatrix} x \\ y \end{Bmatrix} = -\begin{Bmatrix} (1+\mu) \\ \frac{pL}{L_{ee}} \end{Bmatrix} \ddot{z}_b \quad (6)$$

III. NUMERICAL STUDY

For this study a building is modeled as a SDOF structure and a LCVA is mounted on top of the primary structure as shown in Fig. 1, used for the analysis. The properties of primary structure are m =3.0×105

kg, k =8.2247×106 N/m and damping ratio of structures, ξs = 2% .The structure has a natural frequency f1 =0.8333 Hz, which is tuned by frequency of the LCVA. To know the impact of seismic excitations on the performance of LCVA, some past earthquake ground motion records are selected for the analysis. The structure is analyzed twice, once without LCVA and again with a LCVA attached to the top, subjected to past earthquake ground motion records varying with different parameters. The structure without and with LCVA is subjected to previously selected past earthquake data of Park field earthquake (1966), EL-Centro earthquake (1940), Nepal earthquake (2015), and Coalinga earthquake (1983) for different mass ratios.

The variation of displacements of structures with time considering time history data of previously selected earthquakes using LCVA and without damper have been shown in Figs. 2 and Table-1, which shows the effectiveness of the damper in reducing peak structural responses for different mass ratios. The results show that the effectiveness of the LCVA to reduce the structural displacement very significant for some earthquake records and for some records the reductions are not that much effective. For 5% mass ratio and for Parkfield and Coalinga, earthquake data, the peak displacement reductions are 55.91% and 34.70% while for same mass ratio and for EL-Centro and Nepal earthquake data, the reduction are 33.79% and 29.94%.

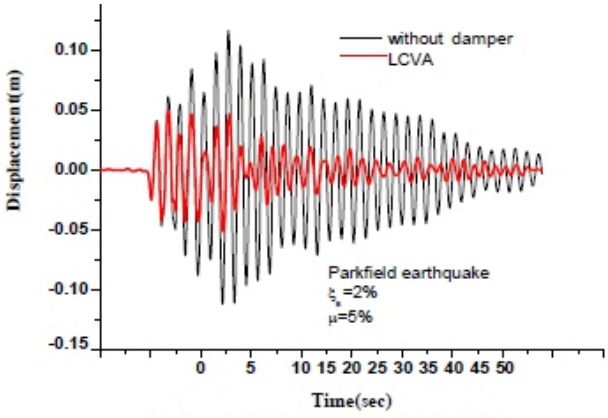

(a) Parkfield earthquake (1966).

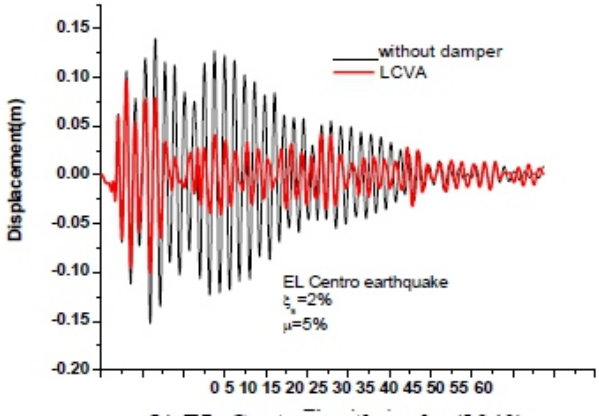

(b) EL-Centro earthquake (1940).

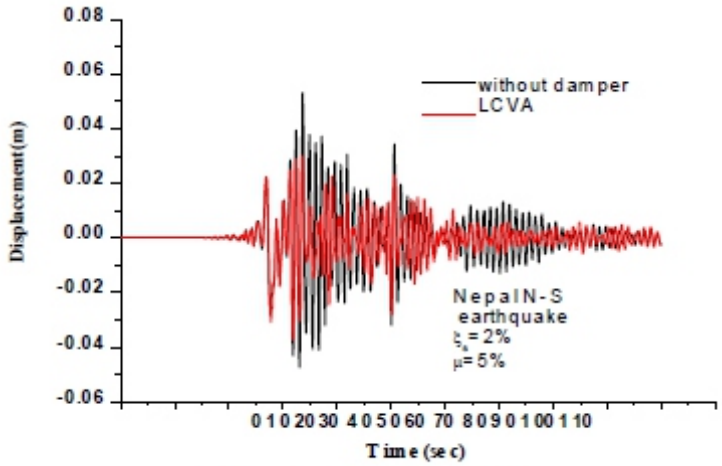

(c)Nepal earthquake (2015).

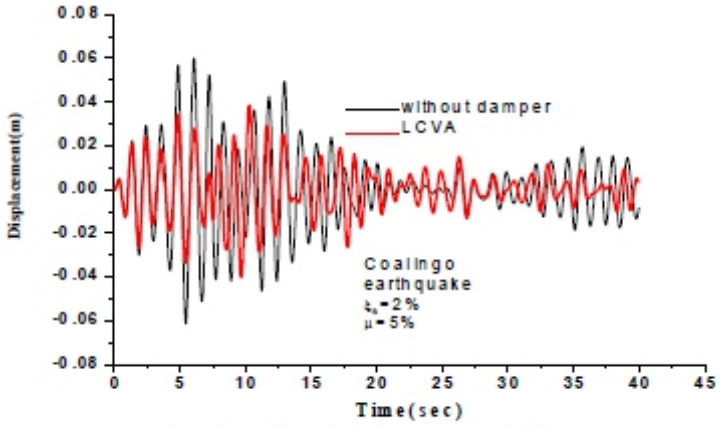

(d) Coalinga earthquake, (1983).

Fig. 2: Variation of displacement of structures considering real time history data of (a) Parkfield earthquake (1966), (b) EL- Centro earthquake (1940), (c)Nepal earthquake (2015),(d) Coalinga earthquake,(1983), for Mass ratio = 5%, Damping ratio of structures=2% and, Length ratio=0.8.

The variation of structural acceleration with time considering time history data of Parkfield earthquake (1966), EL-Centro earthquake (1940), Nepal earthquake (2015), and Coalinga earthquake (1983), with LCVA and without damper are shown in Fig. 3 and Table-2.

From Fig. 3 and Table-2 one can see that peak structural acceleration reduction capacity is not that much significant, this problem is important for acceleration sensitive component, such as non structural components, although this observation needs more extensive analysis for confirmation.

The results also confirm that the effectiveness of the LCVA to reduce structural response is highly dependent upon the nature of the excitations but overall it performs exceptionally well for all earthquakes. From Figs. 2 and 3, it can also be seen that overall structural displacement and acceleration reduction capacity of LCVA is very good.

Table-1: Values of maximum displacement of structure without and with LCVA and corresponding effectiveness of LCVA taking structural damping=2%, frequency tuning ratio=1, blocking ratio=0.1 and length ratio=0.8

Earthquakes	Maximum displacement(m)					% Reduction			
	Without damper	With LCVA Mass ratio				With LCVA Mass ratio			
		1%	3%	5%	7%	1%	3%	5%	7%
Parkfield	0.1168	0.0997	0.0692	0.0515	0.0458	14.64%	40.75%	55.91%	60.79%
El -centro N-S	0.1524	0.1403	0.1189	0.1009	0.094	7.94%	21.98%	33.79%	38.32%
Nepal N-S	0.0531	0.0477	0.0392	0.0372	0.035	10.17%	26.18%	29.94%	34.09%
Coalinga	0.0611	0.0542	0.0424	0.0399	0.0417	11.29%	30.61%	34.70%	31.75%

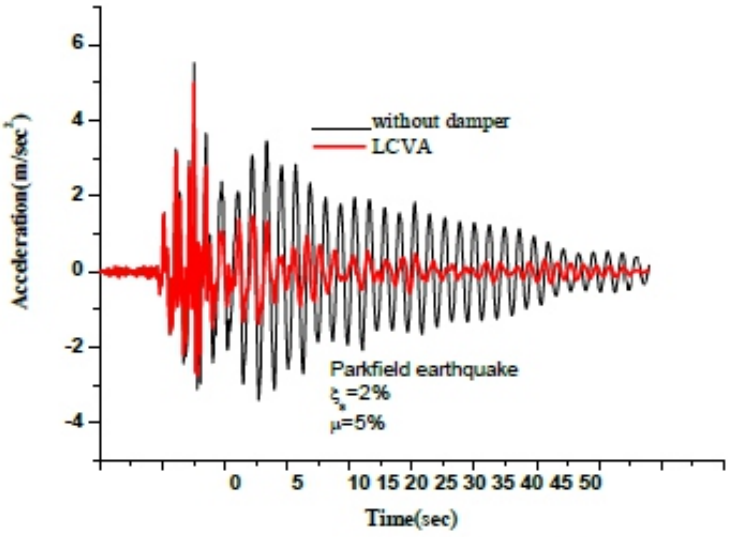

(a) Parkfield earthquake (1966).

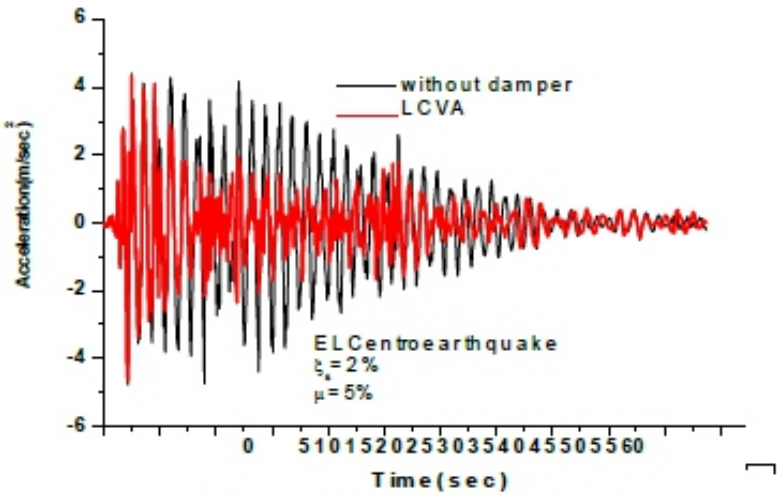

(b) El Centro earthquake (1940).

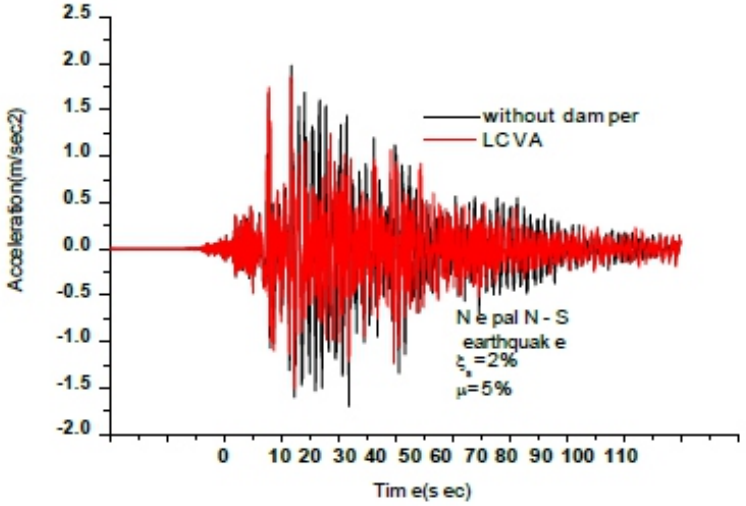

(c)Nepal earthquake (2015).

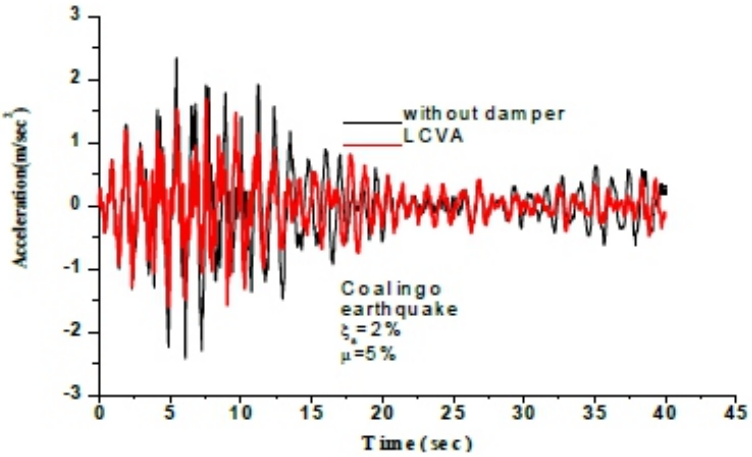

(d) Coalinga earthquake (1983).

Fig. 3: Variation of acceleration of structures considering real time history data of (a) Parkfield earthquake (1966), (b) EL-Centro earthquake (1940), (c) Nepal earthquake (2015), (d) Coalinga earthquake (1983), for mass ratio=5%, Damping ratio of structures=2%, Length ratio=0.8.

Table-2: Values of maximum acceleration of structure without and with LCVA and corresponding effectiveness of LCVA taking structural damping=2%, frequency tuning ratio=1, blocking ratio=0.1 and length ratio=0.8

Earthquakes	Maximum structural acceleration(m/sec^2)					% Reduction			
	Without damper	With LCVA Mass ratio				With LCVA Mass ratio			
		1%	3%	5%	7%	1%	3%	5%	7%
Parkfield	5.5168	5.4011	5.1822	4.9794	4.7919	2.10%	6.07%	9.74%	13.14%
El -centro N-S	4.7706	4.7439	4.6915	4.6403	4.5903	0.56%	1.66%	2.73%	3.78%
Nepal N-S	1.9749	1.9625	1.912	1.8542	1.7878	0.63%	3.18%	6.11%	9.47%
Coalinga	2.4205	2.1784	1.8115	1.6769	1.7203	10.00%	25.16%	30.72%	28.93%

Mass ratio is the most important parameter influencing the effectiveness of LCVA in reducing the structural displacement. It is evident from Table-1 that LCVA with higher mass ratio is more effective in suppressing the structural displacement. To incorporate higher mass and to maintain the liquid column shape the LCVA can consist of small diameter tubes of same length, as the natural frequency of LCVA depends only on its length.

Much higher value of mass ratio is not effective as they add to the inertial load on the structure due to base excitations. Also a higher mass ratio is impractical due to the space requirements.

And much higher mass ratio also increases the overall loading in structures, in real life applications. Fig. 4 shows the influence of length ratio in peak liquid and structural displacement. If the value of length ratio is increased gradually the value of maximum structural displacement is gradually reduced, and the liquid displacement is increasing.

With a higher length ratio LCVA can reduce the maximum structural response more efficiently. This is because the mass of the horizontal part of the LCVA is the only effective mass of LCVA acting on the structure. However length ratio is limited by the liquid displacement bounded values, cause with higher increase of the liquid displacement there is the chance of being out of tuned as a result the efficiency of the LCVA will reduce.

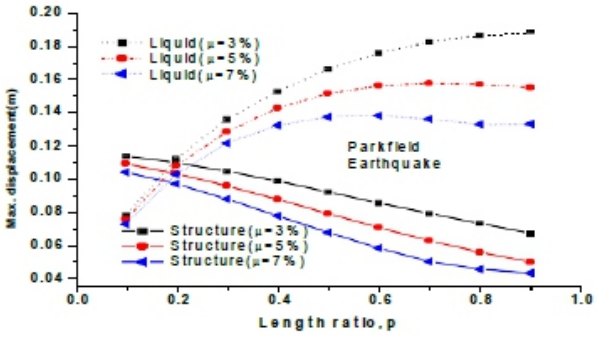

(a) Parkfield earthquake (1966).

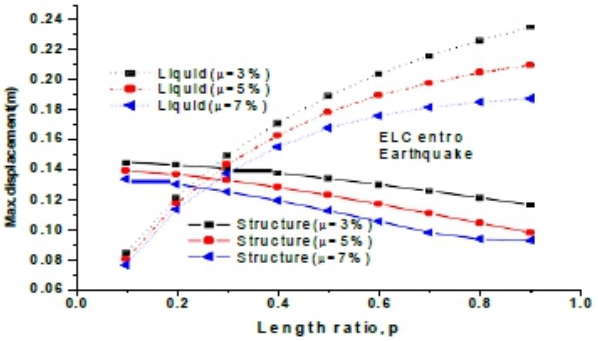

(b) EL-Centro earthquake (1940).

Fig 4: The influence of length ratio on the maximum displacement of structure and liquid for 3% and 5% and 7% mass ratio considering real time history data of (a) Parkfield earthquake, (b) EL-Centro earthquake

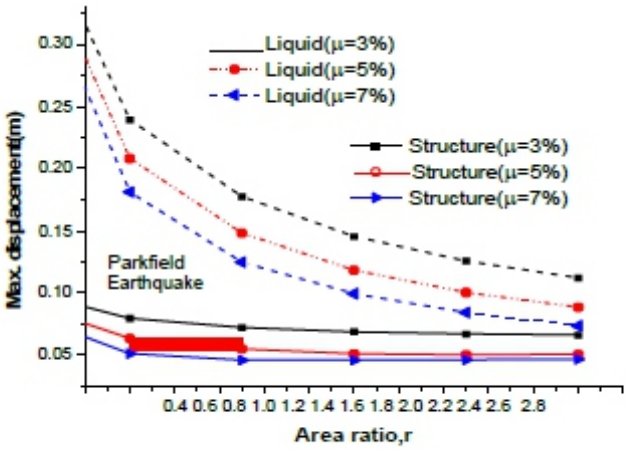

(a) Parkfield earthquake (1966).

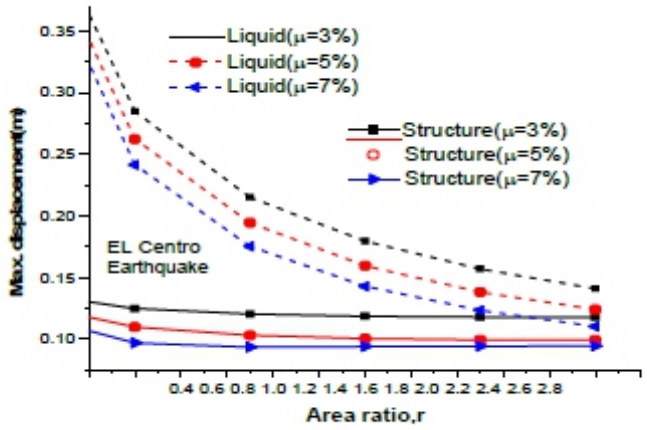

(b) EL-Centro earthquake (1940).

Fig. 5: The influence of area ratio on the maximum displacement of structure and liquid for 3%, 5% and 7% mass ratio considering real time history data of (a) Parkfield earthquake, (b) EL-Centro earthquake

Fig. 5 shows that with increase in area ratio the liquid displacement as well as the structural displacement is decreasing. As the liquid and structural displacement decreasing, the efficiency of LCVA will increase and there is less chance of being out of tuned and could be a possible advantage when headroom is restricted. Moreover from Fig. 4 and Fig. 5 it can be concluded that in the range of length ratio 0.7 to 0.8 and area ratio 1.5 to 2 the LCVA is more efficient.

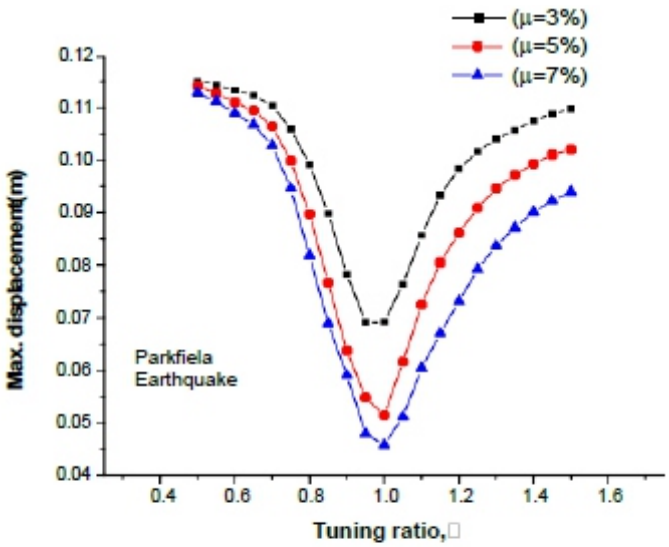

(a) Parkfield earthquake (1966).

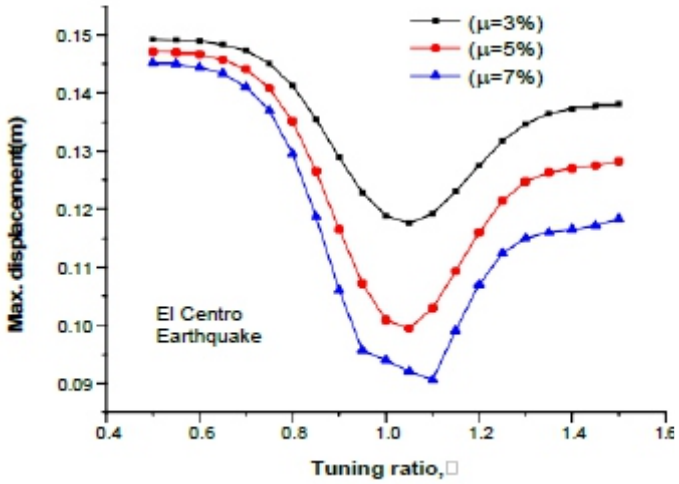

(b) EL-Centro earthquake (1940).

Fig. 6: Variation of max. Displacement of structures with tuning ratio for 2% damping ratio and 3%, 5% and 7% mass ratio considering real time history data of (a) Parkfield, (b) EL-Centro earthquake.

It is very important that LCVA should be tuned properly with the structural frequency for better performance. The optimal tuning ratio not only depends upon the mass ratio and the damping of structure but also depends upon the nature of the excitations. Although the influence of the tuning ratio on the effectiveness of the damper is different for different earthquake nature, and slightly change with the change of mass ratio, still, it can be seen from Fig. 6 that in the range of tuning ratio, γ 0.9 to 1.1 the LCVA is more efficient in controlling the structural response.

CONCLUSIONS

The result of the study shows that with the proper design parameters LCVA is efficient to reduce peak structural displacement due to the seismic excitations while the peak acceleration reduction capacity is comparatively less, but overall structural displacement and acceleration capacity is very efficient. The study also shows that the parameters1. play significant role to the performance of the LCVA and some of the parameters are also sensitive to the nature of the excitations, some similarities is found in the nature of the behavior of the damper due to different type of earthquake excitations, which is very helpful in designing the damper for real life applications. Although the structural displacement and acceleration reduction capacity of LCVA are highly depends on the nature of the excitation but overall it performs exceptionally well for all earthquakes, by standing out the maximum structural displacements and also rapid response decay. This is very beneficial in real life, by enhancing occupants comfort and safety in flexible building with low intrinsic structural damping.

REFERENCES

[1] Sakai F, Takaeda S. Tamaki T. [1989] "Tuned liquid column damper – new type device for suppression of building vibration," Proceedings of the International Conference on High-rise Buildings, Nanjing, China, pp. 926-931.

[2] Watkins, R. D. [1991] "Tests on a liquid column vibration absorber for tallstructures", Proc. Int. Conf on Steel and Aluminium Structures, Singapore,

[3] C.C Chang, C.T. Hsu [1998] "Control performance of liquid column vibration absorber", Engineering Structures, 20(7), 580-586.

[4] Wu, J.-C., Shih, M-H., Lin, Y-Y, Shen, Y-C. [2005] "Design guidelines for tuned liquid column damper for structures responding to wind," Engineering Structures 27, 1893-1905.

[5] Chakraborty, S., Debbarma, R. [2011] "Stochastic earthquake response control of structure by liquid column vibration absorber with uncertain bounded system parameters," Structural Safety, 33,136-144.

Hourly Rainfall Generation by Markov Chain Rainfall Generator

Ujjwal Saha
[1]Civil Engineering Department, IIEST Shibpur, Howrah-3
E-mail: 1ujjwalsaha1980@gmail

ABSTRACT

Simulation of hourly rainfall is very important in urban hydrology and small catchments with fast concentration time to model the hydrological processes and prediction of flash flood. Considerable efforts have been given to simulate the daily rainfall but there is not much research on modeling of hourly rainfall. Most hourly rainfall simulation model is based on poisson cluster theory which requires large number of parameters to be estimated and the parameter estimation procedure is complex. To overcome this problem, in this study, a first order two state Markov chain rainfall generator with gamma distribution is used to simulate hourly rainfall of a station in the city of Kolkata. The results indicate that the model is successful to simulate the diurnal cycle of rainfall with an acceptable degree of accuracy but need further improvement.

Keywords- Hourly Rainfall Generator, Markov Chain, Transitional Probabilities, Diurnal Cycle

I. INTRODUCTION

To combat the flooding in urban areas, storm water drains are constructed. The urban storm water systems are designed based on extreme rainfall amount for the return period equal to the expected life of the system and duration of rainfall is equal to the time of concentration of the urban watershed for which the storm water systems are to be designed. As variability of various hydrological, topographical and social parameters is high in an urban area, typically urban storm water facilities are designed for small catchment areas. The time of concentration falls between 45 minutes to 1 hour. Sometimes it can be as low as 15 minutes (Mailhot and Duchesne 2010). Frequency analysis of rainfall data for the appropriate durations has to be performed to get the required design rainfall. But, in developing countries such as India, the availability of short duration rainfall data is scarce. Sometimes, the hourly data will have missing values. Hence, simulation of hourly data is extremely important area but unfortunately not much effort is spent in this area. In this study, an effort has been made to simulate the hourly rainfall of a station in Kolkata city, India.

The simulation of hourly rainfall follows four broad methods. In first set of method, at first daily rainfall is simulated and then the daily rainfall values are disaggregated into hourly values by different techniques such as Random Cascade, scaling theory. Second set of method model the rainfall as Poisson cluster process. The Bartlett-Lewis and Neyman- Scott pulse processes (Rodriguez-Iturbe et al., 1987

and 1998) are the two predominant model variants in this category. Cluster process models provide occurrence and amount in the same model (Koutsoyiannis and Onof, 2001). Both models are based on Poisson process of arrival of storm origins with each origin associated with a random number of cells. In the Neyman Scott process, the positions of the cells are determined from the storm origin assuming it as an independent and identically distributed. On the other hand, in the Barlett-Lewis process, the intervals between consecutive cells are assumed to be independent and identically distributed. In both cluster based models, it is assumed that the placement of cells is governed by an exponential distribution that characterizes either the positioning of cells from the storm origin (NSRP case) or the inter-arrival time between cells (BLRP case). The main problem with cluster process models is that of parameterization. Studies (e.g., Cowpertwait et al., 2002) have noted that cluster process rainfall models break down or reveal lack of fit at certain temporal or spatial scales The third method, non-parametric rainfall generators, have evolved as a simple way to simulate rainfall data while avoiding the statistical assumptions regarding the probability distributions of rainfall. Most of the existing algorithms are extensions of the Young (1994) approach, using a nearest-neighbor resampling scheme in selection of the next time scale weather. The fourth category of method is called chain dependant process and most popular in this category is Markov chain rainfall generators. A Markov chain may be thought as a collection of states of a system. For each time period the state of the Markov chain can either continue in the same state or move into another state (Wilks, 1999). For modeling of the rainfall occurrence, the Markov chain approach is generally limited to two states: rainy or dry. The behavior of a Markov chain is governed by conditional probabilities known as transition probabilities. A transition probability is the probability of going from a given state to the next state in a Markov chain.

There is only one significant work of applying the Markov chain process in simulation of hourly rainfall (Katz, 1995). The authors assumed dependency between successive rainfall amounts by an autoregressive model which made the model complicated. In this work, It is assumed that rainfallamount of different hours in a day will be independent to each other. The methodology of the simulation process is described in the next section. In the third section, the results of the output of the model is presented and discussed. Finally in the last section, conclusions are drawn.

II.SIMULATION PROCESS

The hourly rainfall is simulated in a two step process. In the first step, the rainfall occurrence i.e sequence of dry and wet hours is simulated and in the next step, the rainfall amount on the wet hours is simulated. For simulating rainfall occurrence, the hourly rainfall process is assumed as an random variable { RSd(h) ; h = 1,2 3 to 24 and d is 1,2… D where D is the total length of the daily time series} is defined as RSd(h)= 0 if there is no rainfall occurrence on that h th hour of d th day RSd(h) = 1 if there is

rainfall occurrence Assuming that the random function, R(t) evolves as a function of its previous state and it follows Markovian dependence of first order,

$$P[RS_d(h) = 1 | RS_d(h-1), RS_d(h-2), \ldots RS_d(1)]$$
$$= P[RS_d(h) = 1 | RS_d(h-1)] \quad (1)$$

The generation of the states 0 and 1 of R(t) requires the specification of conditional or transition probabilities. As the random variable R(t) have two state space, it will have a transition probability matrix of 2 × 2 in the form of

$$p_{00} = P[RS_d(h) = 0 | RS_d(h-1) = 0]$$
$$p_{01} = P[RS_d(h) = 0 | RS_d(h-1) = 1]$$
$$p_{10} = P[RS_d(h) = 1 | RS_d(h-1) = 0]$$
$$p_{11} = P[RS_d(h) = 1 | RS_d(h-1) = 1] \quad (2)$$

As there is only two possible state in a particular hour, it follows that the transition probabilities are related by

$$p_{10} = 1 - p_{11}$$
$$p_{01} = 1 - p_{00} \quad (3)$$

Hence, the transition probability matrix can be defined if only two transition probabilities, p01 and p11 is estimated from the observed data. The conditional probabilities can be estimated from the observed conditional frequency of rainfall state transition as follows:

		Current hour		
Previous hour		Dry	Rain	Total
	Dry	N00	N01	Nd
	Rain	N10	N11	Nr

Where N00, N01, N10 and N11 are the observed frequencies:

N00 = Number of dry hours preceded by dry hours

N01 = Number of rain hours preceded by dry hours

N10 = Number of dry hours preceded by rain hours

N11 = Number of rain hours preceded by rain hours

And N00 + N01 = Nd, total number of dry hours

N10 + N11 = Nr, total number of rain hours

Now the maximum likelihood estimator for the transition probabilities are

$$p_{ij} = \frac{Nij}{Nt} \quad \text{for i, j = 1,2} \quad (4)$$

Here in order to take seasonal characteristics of rainfall into account, the transitional probabilities are calculated for each month. This improves the intra-annual representation of the random variable RSd(h).

Once the rainfall occurrence process is simulated, next step is to simulate the rainfall amount (Ra) in each wet hour. The rainfall amount generation process is done fitting Gamma distribution to wet hours.

The daily rainfall amount 'x' on wet hour is described by a Gamma distribution with probability function

$$f(x) = \frac{\left(x/\beta\right)^{\alpha-1} \exp\left(-x/\beta\right)}{\beta\Gamma(\alpha)} \quad ; \ \alpha, \beta > 0; \quad x > 0 \qquad (5)$$

where α is the shape parameter, and β is the scale parameter, Γ(α) is the Gamma function. The parameters of Gamma distributions are estimated by maximum likelihood method . After the transition probabilities and Gamma distribution parameters for each month are estimated from the observed data, the dry-rain status of each hour needs to be established. For determining dryrain status of the first hour of the day, a uniform random number is generated; if this random number is greater than 0.5, then the day is taken as dry, otherwise it is considered as a wet. To determine whether the next hour of the sequence is rain or dry, critical value of probability, Pcrit, of rainfall is calculated. It depends on the dry or rain status of the previous hour. If the previous hour is dry, then Pcrit= p01 otherwise Pcrit= p11. Again another uniform random number (u) is generated. The current hour is simulated as dry if u > Pcrit otherwise it is a wet hour. This procedure continues for all remaining days of the year.

After rainfall status of each hour is determined, next step is to simulate the rainfall amounts in each hour. This is done by monte-carlo simulation. Again, a uniform random number is generated between 1 and 0. This random number is assumed to be CDF of the respective Gamma distribution (equation (5)). The rainfall amount is obtained by setting the CDF equal to the uniform random number and solving the CDF. Thus the hourly rainfall for each hour is simulated. Since the model uses a random number, every time the model is run it gives a different result. To tackle this issue, the model is run 100 times and the mean of the statistics is taken as simulated. Note that in this study, it is the statistical properties of rainfall which is more important than the exact sequence of rainfall, and a rainfall generator is designed for that purpose.

III. RESULTS AND DISCUSSION

At first it was decided that how many runs of the algorithm are required so that the results converge. In the following figure 1, it can be observed that after at around 100 runs, results seem to be converging.

Hence, in this study, it is decided to run the model for 100 times to get the average of the statistical parameters.

At first, the parameters of the models are calculated. In order to investigate further, four types of model have been used in this model. Case1: The model parameters (i.e. Transition probabilities p01 and p11 and gamma distribution parameters α and β) are not allowed to vary diurnally. Case2: The Transition probabilities are not allowed to vary diurnally while gamma distribution parameters are varied diurnally. Case3: All the parameters are allowed to vary diurnally

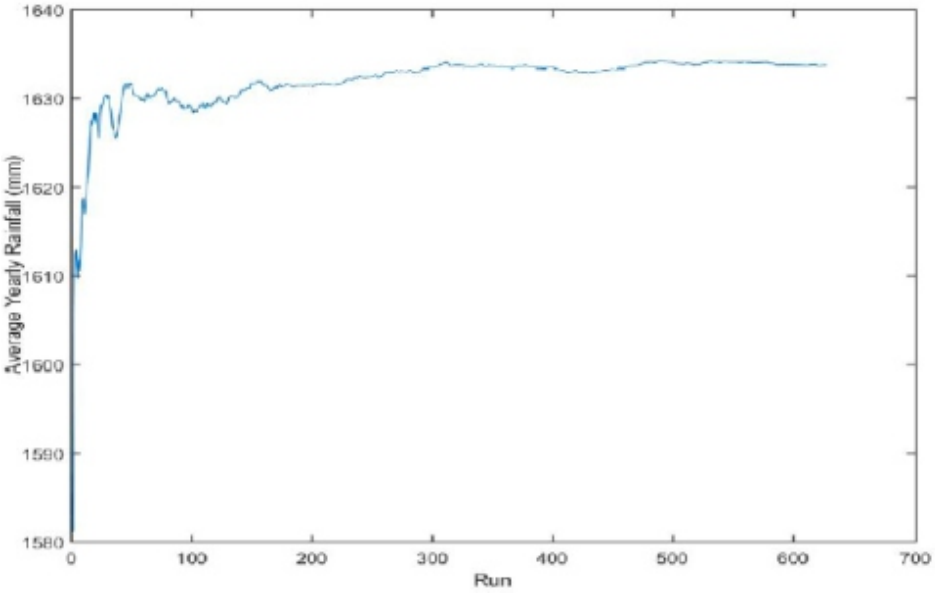

The calculated parameters of the model in all the cases are given below.

Table1: Model Parameters of Dumdum Station assuming no Diurnal Variation

Month	P01	P11	alpha	beta
Jan	0.004	0.627	0.73	2.02
Feb	0.007	0.516	0.57	4.17
Mar	0.008	0.490	0.54	5.97
Apr	0.011	0.490	0.53	6.80
May	0.021	0.565	0.50	9.05
Jun	0.052	0.580	0.52	6.45
July	0.078	0.570	0.52	5.56
Aug	0.076	0.558	0.54	5.65
Sept	0.056	0.596	0.54	6.07
Oct	0.022	0.614	0.54	6.15
Nov	0.006	0.690	0.57	4.68
Dec	0.002	0.671	0.57	3.34

Table2: Model Parameter (Alpha) of Dumdum Station with Hourly Variation

Month	1	2	3	4	5	6	7	8	9	10	11	12	13	14	15	16	17	18	19	20	21	22	23	24
Jan	0.72	0.64	1.08	0.57	1.03	0.66	0.69	0.82	1.12	0.53	0.54	0.80	1.16	0.73	0.70	0.64	0.69	1.14	0.88	1.10	0.63	0.82	1.65	1.02
Feb	0.58	0.69	0.55	0.39	0.61	0.53	0.73	0.93	1.08	3.91	0.50	1.03	0.52	0.82	0.70	0.79	0.52	0.83	0.64	0.57	0.65	0.86	0.63	0.50
Mar	0.52	0.48	0.69	0.41	0.66	0.87	0.62	1.25	0.46	0.87	0.40	0.64	0.83	0.51	0.74	0.65	0.54	0.70	0.54	0.61	0.52	0.59	0.63	0.49
Apr	0.45	0.79	0.45	0.37	0.60	0.52	0.58	0.46	1.17	0.61	0.49	1.00	0.55	0.91	0.48	0.66	0.46	0.61	0.52	0.57	0.56	0.70	0.55	1.10
May	0.56	0.66	0.47	0.46	0.45	0.41	0.65	0.50	0.99	0.66	0.42	0.50	0.65	0.50	0.62	0.46	0.40	0.53	0.54	0.52	0.52	0.47	0.53	0.59
Jun	0.47	0.51	0.76	0.59	0.57	0.60	0.54	0.53	0.63	0.62	0.53	0.52	0.58	0.56	0.52	0.55	0.52	0.46	0.50	0.45	0.46	0.42	0.46	0.47
July	0.46	0.54	0.57	0.63	0.54	0.55	0.52	0.48	0.59	0.52	0.53	0.62	0.51	0.61	0.48	0.52	0.52	0.49	0.53	0.57	0.48	0.53	0.46	0.47
Aug	0.51	0.49	0.50	0.51	0.63	0.54	0.57	0.58	0.58	0.67	0.65	0.59	0.53	0.49	0.53	0.57	0.51	0.51	0.47	0.59	0.51	0.56	0.52	0.59
Sept	0.57	0.56	0.55	0.53	0.61	0.64	0.55	0.55	0.61	0.63	0.67	0.55	0.53	0.58	0.50	0.54	0.48	0.53	0.47	0.44	0.49	0.50	0.51	0.54
Oct	0.60	0.47	0.57	0.69	0.60	0.58	0.59	0.45	0.63	0.70	0.56	0.48	0.55	0.68	0.64	0.50	0.45	0.48	0.49	0.49	0.52	0.56	0.61	0.65
Nov	0.52	0.42	0.49	0.51	0.70	0.70	0.56	0.62	0.69	0.62	0.76	0.64	0.70	0.74	0.62	0.66	0.58	0.55	0.94	0.56	0.75	0.69	0.60	0.67
Dec	0.43	0.70	0.33	0.68	0.67	0.99	1.07	0.82	0.58	1.41	1.97	1.62	1.69	1.19	1.84	0.80	0.61	0.52	0.62	0.35	0.36	0.42	0.36	0.45

Table3: Model Parameter (Beta) of Dumdum Station with Hourly Variation

Month	1	2	3	4	5	6	7	8	9	1	11	12	1	14	1	16	17	18	19	20	21	22	23	24
Jan	1.98	2.50	1.22	4.79	1.69	1.84	2.63	2.43	1.20	3.56	3.11	1.03	0.79	1.27	2.87	2.04	1.82	0.66	2.03	1.46	1.90	1.25	0.37	1.43
Feb	5.60	3.63	3.20	4.69	5.73	5.30	1.85	1.20	0.58	0.08	6.38	2.68	5.74	2.95	4.91	2.94	10.28	0.84	3.48	5.78	2.99	1.34	3.22	5.01
Mar	6.89	8.14	1.67	9.99	2.26	2.21	6.30	0.41	6.61	1.56	12.66	2.06	1.74	9.14	5.66	8.49	8.71	2.63	8.78	5.31	7.72	4.14	5.44	6.38
Apr	9.30	2.49	7.35	14.66	2.04	5.12	3.94	6.31	10.16	6.13	3.23	2.16	7.58	2.03	7.76	2.75	10.76	7.54	10.76	6.74	4.41	3.22	5.62	1.93
May	4.98	3.82	6.40	5.91	5.46	13.27	5.35	7.58	2.17	3.58	10.63	9.56	7.78	11.45	6.90	12.23	21.69	12.59	11.78	8.59	7.26	8.48	6.32	3.25
Jun	8.16	5.76	2.23	4.46	5.56	5.24	4.76	6.29	5.17	4.01	7.44	6.12	4.66	5.91	6.58	5.72	7.84	9.43	7.44	10.09	6.94	10.95	5.78	7.84
July	7.76	4.92	3.86	3.79	5.62	4.90	5.95	5.08	3.79	5.25	4.49	3.98	7.05	5.13	8.18	6.33	5.28	7.06	6.29	4.27	6.33	4.21	6.20	5.59
Aug	7.82	7.58	7.67	6.67	4.66	5.42	4.02	3.50	4.61	3.25	3.37	5.22	6.27	7.84	7.69	5.00	6.27	5.40	6.93	3.74	5.16	4.29	5.81	4.25
Sept	4.81	5.22	4.74	6.56	4.45	4.74	5.11	6.06	3.58	4.78	3.54	7.69	9.54	6.77	6.95	4.85	6.80	4.17	7.02	8.58	6.34	5.83	7.42	7.21
Oct	5.52	8.64	5.46	3.11	5.49	5.66	5.12	8.39	4.50	4.93	6.65	10.40	9.20	4.77	5.87	7.06	8.55	6.53	5.06	4.54	4.44	3.57	2.68	3.60
Nov	5.03	11.23	8.77	5.33	2.55	1.90	4.21	4.13	2.36	4.62	5.79	3.67	5.34	3.75	4.58	3.39	3.79	5.40	1.47	5.84	1.43	4.92	2.77	2.35
Dec	6.18	1.68	23.27	2.58	2.36	2.93	1.48	1.04	2.42	1.35	0.39	0.56	0.53	0.72	0.47	1.78	2.43	3.64	1.65	6.33	10.67	6.11	9.71	4.22

Table4: Model Parameter (p11) of Dumdum Station with Hourly Variation

Month	1	2	3	4	5	6	7	8	9	10	11	12	13	14	15	16	17	18	19	20	21	22	23	24
Jan	0.58	0.58	0.52	0.73	0.82	0.57	0.64	0.56	0.56	0.50	0.75	0.36	0.85	0.90	0.50	0.71	0.37	0.77	0.63	0.91	0.53	0.54	0.55	0.66
Feb	0.61	0.59	0.42	0.50	0.50	0.43	0.45	0.30	0.44	0.60	0.54	0.83	0.42	0.46	0.50	0.46	0.47	0.58	0.42	0.73	0.47	0.47	0.55	0.52
Mar	0.58	0.47	0.50	0.62	0.56	0.61	0.28	0.50	0.53	0.46	0.50	0.62	0.45	0.61	0.50	0.40	0.50	0.40	0.46	0.47	0.51	0.34	0.66	0.34
Apr	0.66	0.46	0.54	0.52	0.31	0.43	0.44	0.07	0.62	0.30	0.50	0.72	0.29	0.55	0.47	0.41	0.46	0.61	0.52	0.46	0.45	0.55	0.40	0.62
May	0.66	0.63	0.68	0.44	0.61	0.51	0.73	0.40	0.63	0.65	0.71	0.67	0.45	0.63	0.64	0.48	0.59	0.59	0.64	0.56	0.52	0.44	0.48	0.36
Jun	0.67	0.62	0.57	0.63	0.61	0.65	0.65	0.52	0.56	0.63	0.59	0.59	0.61	0.56	0.47	0.54	0.56	0.50	0.59	0.56	0.51	0.65	0.58	0.51
July	0.60	0.67	0.61	0.59	0.64	0.65	0.63	0.48	0.61	0.59	0.58	0.55	0.49	0.55	0.49	0.49	0.49	0.56	0.59	0.57	0.55	0.59	0.59	0.54
Aug	0.65	0.66	0.60	0.64	0.62	0.59	0.61	0.54	0.62	0.57	0.54	0.61	0.49	0.50	0.53	0.51	0.46	0.48	0.46	0.47	0.50	0.59	0.63	0.58
Sept	0.64	0.67	0.73	0.70	0.71	0.69	0.62	0.58	0.66	0.63	0.60	0.60	0.58	0.57	0.53	0.45	0.51	0.48	0.49	0.55	0.62	0.58	0.62	0.61
Oct	0.70	0.64	0.69	0.69	0.74	0.60	0.76	0.60	0.55	0.66	0.69	0.60	0.61	0.48	0.58	0.49	0.61	0.52	0.55	0.67	0.62	0.57	0.62	0.63
Nov	0.85	0.83	0.54	0.67	0.60	0.68	0.52	0.52	0.88	0.60	0.83	0.58	0.68	0.78	0.54	0.57	0.72	0.69	0.71	0.72	0.61	0.91	0.93	0.78
Dec	0.58	0.50	0.66	0.66	0.61	0.72	0.66	0.66	0.66	0.66	0.75	0.75	0.66	0.62	0.71	0.57	0.75	0.50	0.71	0.85	0.71	0.71	0.85	0.75

Using these parameters, the model is run for 100 times and the hourly rainfall time series are generated and then the various rainfall statistics are calculated and compared with the observed. The results are shown below.

Case 1:

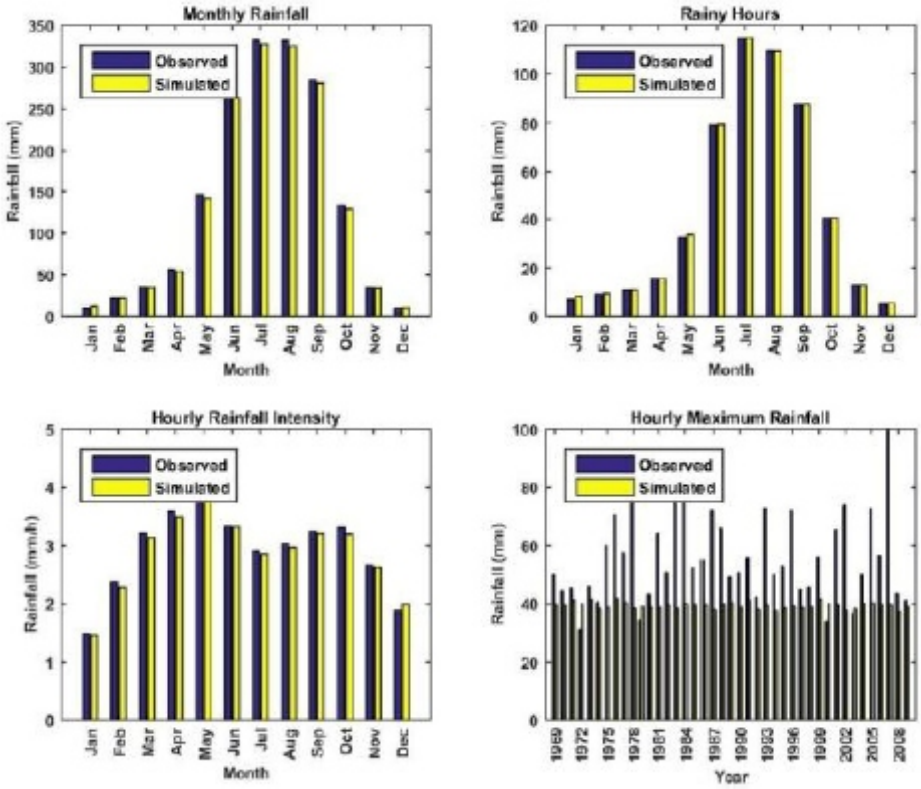

Figure 2: Monthly Rainfall Simulation

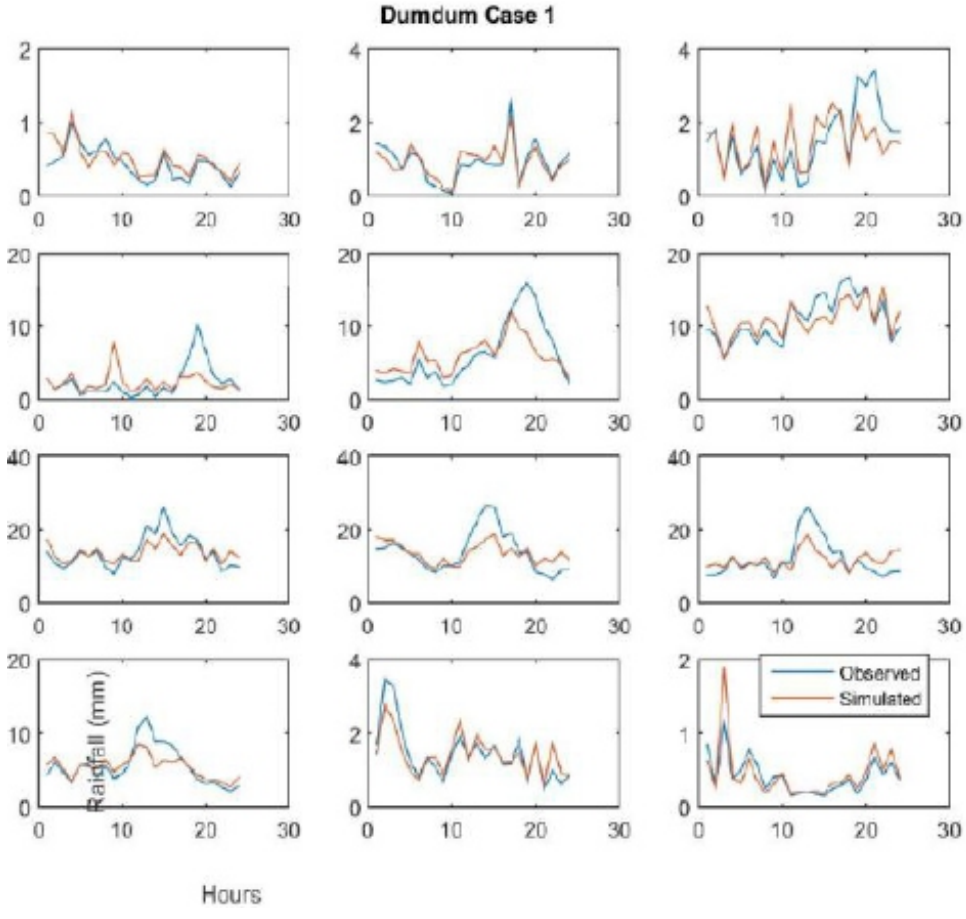

Figure 3: Duirnal Rainfall Simulation

Case 2:

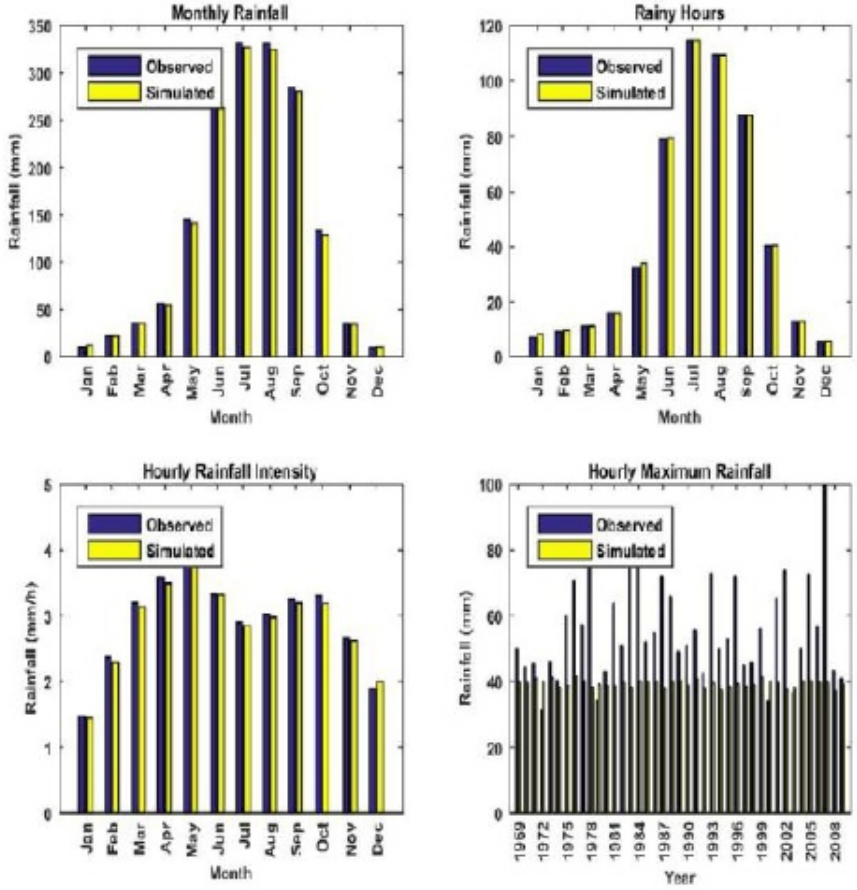

Figure 4: Monthly Rainfall Simulation

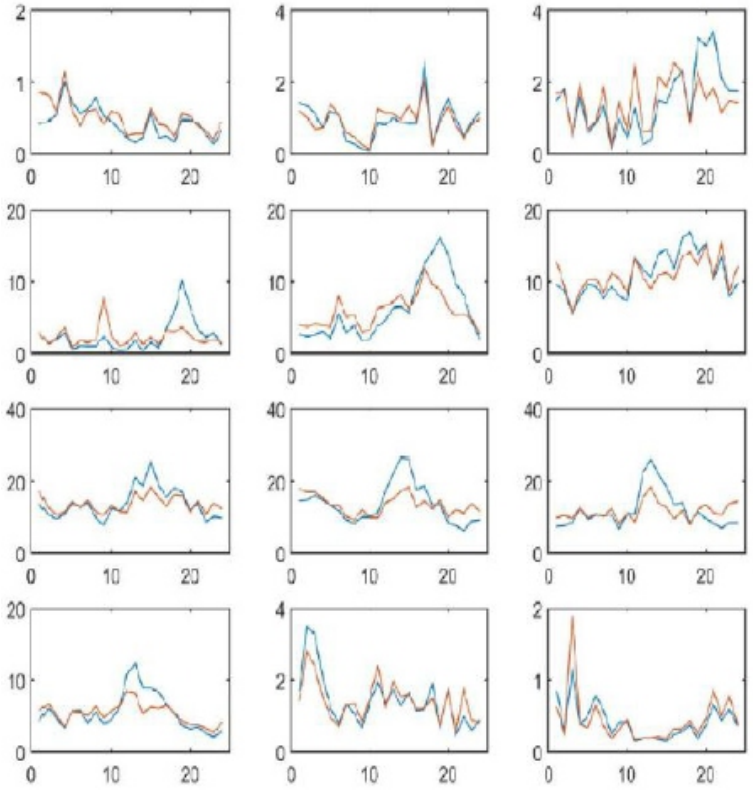

Figure 5: Duirnal Rainfall Simulation

Case 3:

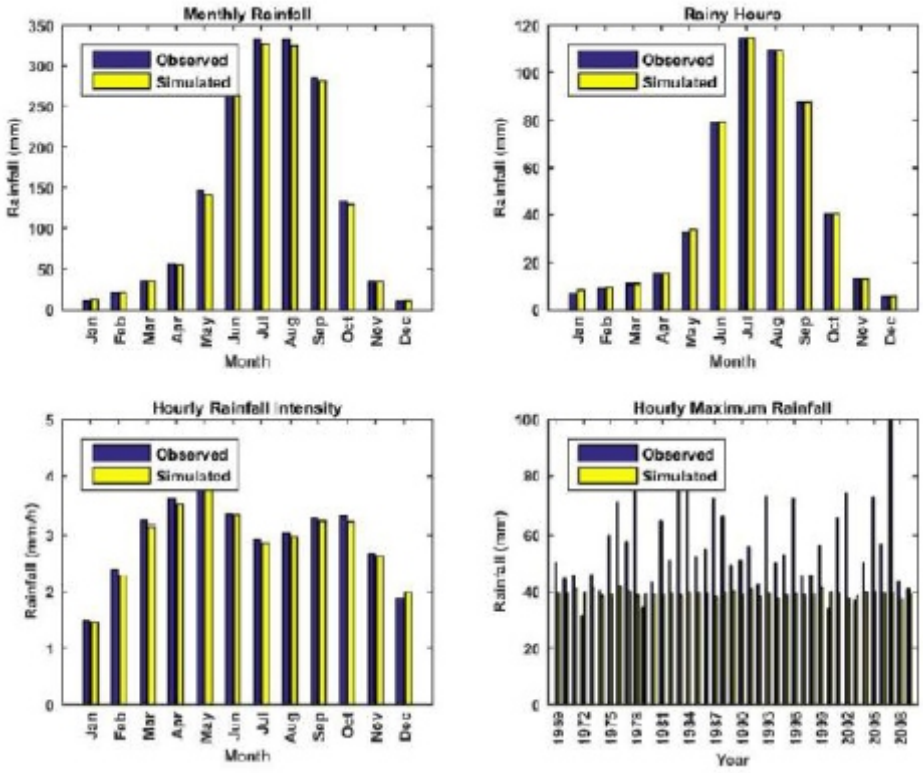

Figure 6: Monthly Rainfall Simulation

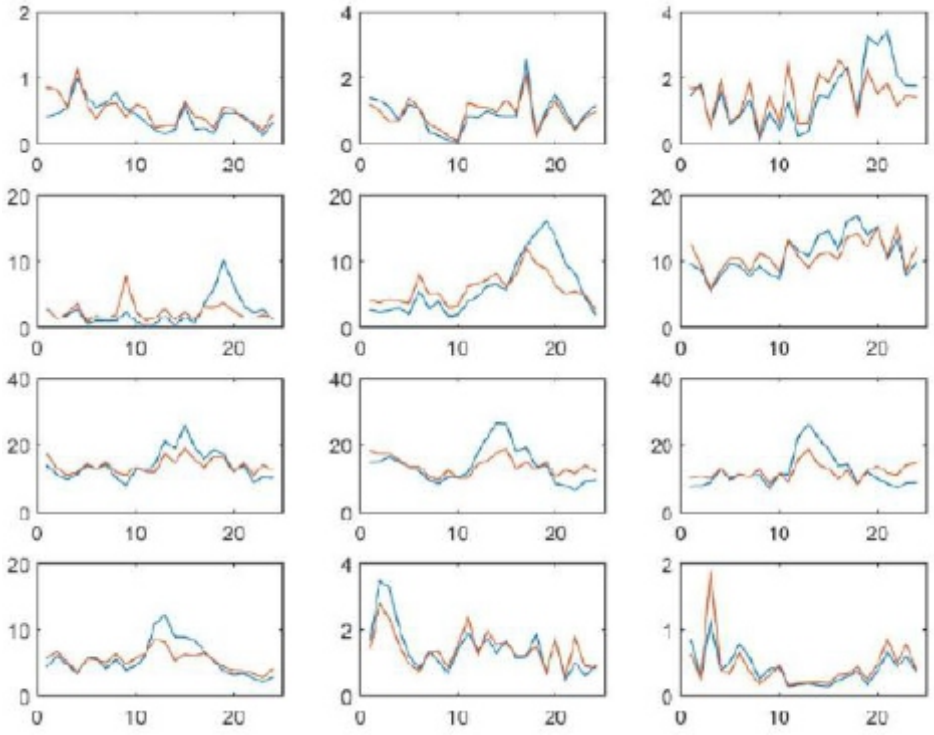

Figure 7: Duirnal Rainfall Simulation

CONCLUSIONS

The hourly rainfall distribution and various statistics of rainfall at different aggregation level are simulated with desired accuracy by this markov chain model but the extreme rainfall statistics is not simulated well. Hence, improvement of this model is necessary.

REFERENCES

[1] Cowpertwait, P. S. P., Kilsby, C. G., and O'Connell, P. E. (2002), A spacetime NeymanScott model of rainfall: Empirical analysis of extremes, Water Resources Research, 38(8), 6-11.

[2] Katz, R. W., & Parlange, M. B. (1995). Generalizations of chain-dependent processes: Application to hourly precipitation. Water Resources Research, 31(EFLUM- ARTICLE-1995-007), 1331-1341.

[3] Koutsoyiannis, D., and C. Onof (2001), Rainfall disaggregation using adjusting procedures on a Poisson cluster model, Journal of Hydrology, 246, 109–122.

[4] Mailhot, A., and Duchesne, S. (2010), Design criteria of urban drainage infrastructures under climate change, J. Water Resour. Plann.Manage., 136(2), 201–208

[5] Rodriguez-Iturbe, I., Cox, D. R., Isham, V. (1987), Some models for rainfall based on stochastic point processes, Proc. R. Soc. Lond. A, 410, 269-298.

[6] Rodriguez-Iturbe, I., Cox, D. R., Isham, V. (1988), A point process model for rainfall: Further developments, Proc. R. Soc. Lond. A, 417, 283-298.

[7] Wilks, D. S., and Wilby, R. L. (1999), The weather generator game: a review of stochastic weather models, Prog. Phys. Geogr., 23, 329–358.

[8] Young, K. C. (1994), A multivariate chain model for simulating climatic parameters from daily data, Journal of Applied Meteorology, 33, 661–71.

Instructions for Authors

Essentials for Publishing in this Journal

1 Submitted articles should not have been previously published or be currently under consideration for publication elsewhere.

2 Conference papers may only be submitted if the paper has been completely re-written (taken to mean more than 50%) and the author has cleared any necessary permission with the copyright owner if it has been previously copyrighted.

3 All our articles are refereed through a double-blind process.

4 All authors must declare they have read and agreed to the content of the submitted article and must sign a declaration correspond to the originality of the article.

Submission Process

All articles for this journal must be submitted using our online submissions system. http://enrichedpub.com/ . Please use the Submit Your Article link in the Author Service area.

Manuscript Guidelines

The instructions to authors about the article preparation for publication in the Manuscripts are submitted online, through the e-Ur (Electronic editing) system, developed by **Enriched Publications Pvt. Ltd**. The article should contain the abstract with keywords, introduction, body, conclusion, references and the summary in English language (without heading and subheading enumeration). The article length should not exceed 16 pages of A4 paper format.

Title

The title should be informative. It is in both Journal's and author's best interest to use terms suitable. For indexing and word search. If there are no such terms in the title, the author is strongly advised to add a subtitle. The title should be given in English as well. The titles precede the abstract and the summary in an appropriate language.

Letterhead Title

The letterhead title is given at a top of each page for easier identification of article copies in an Electronic form in particular. It contains the author's surname and first name initial .article title, journal title and collation (year, volume, and issue, first and last page). The journal and article titles can be given in a shortened form.

Author's Name

Full name(s) of author(s) should be used. It is advisable to give the middle initial. Names are given in their original form.

Contact Details

The postal address or the e-mail address of the author (usually of the first one if there are more Authors) is given in the footnote at the bottom of the first page.

Type of Articles

Classification of articles is a duty of the editorial staff and is of special importance. Referees and the members of the editorial staff, or section editors, can propose a category, but the editor-in-chief has the sole responsibility for their classification. Journal articles are classified as follows:

Scientific articles:

1. Original scientific paper (giving the previously unpublished results of the author's own research based on management methods).

2. Survey paper (giving an original, detailed and critical view of a research problem or an area to which the author has made a contribution visible through his self-citation);

3. Short or preliminary communication (original management paper of full format but of a smaller extent or of a preliminary character);

4. Scientific critique or forum (discussion on a particular scientific topic, based exclusively on management argumentation) and commentaries. Exceptionally, in particular areas, a scientific paper in the Journal can be in a form of a monograph or a critical edition of scientific data (historical, archival, lexicographic, bibliographic, data survey, etc.) which were unknown or hardly accessible for scientific research.

Professional articles:

1. Professional paper (contribution offering experience useful for improvement of professional practice but not necessarily based on scientific methods);
2. Informative contribution (editorial, commentary, etc.);
3. Review (of a book, software, case study, scientific event, etc.)

Language

The article should be in English. The grammar and style of the article should be of good quality. The systematized text should be without abbreviations (except standard ones). All measurements must be in SI units. The sequence of formulae is denoted in Arabic numerals in parentheses on the right-hand side.

Abstract and Summary

An abstract is a concise informative presentation of the article content for fast and accurate Evaluation of its relevance. It is both in the Editorial Office's and the author's best interest for an abstract to contain terms often used for indexing and article search. The abstract describes the purpose of the study and the methods, outlines the findings and state the conclusions. A 100- to 250- Word abstract should be placed between the title and the keywords with the body text to follow. Besides an abstract are advised to have a summary in English, at the end of the article, after the Reference list. The summary should be structured and long up to 1/10 of the article length (it is more extensive than the abstract).

Keywords

Keywords are terms or phrases showing adequately the article content for indexing and search purposes. They should be allocated heaving in mind widely accepted international sources (index, dictionary or thesaurus), such as the Web of Science keyword list for science in general. The higher their usage frequency is the better. Up to 10 keywords immediately follow the abstract and the summary, in respective languages.

Acknowledgements

The name and the number of the project or programmed within which the article was realized is given in a separate note at the bottom of the first page together with the name of the institution which financially supported the project or programmed.

Tables and Illustrations

All the captions should be in the original language as well as in English, together with the texts in illustrations if possible. Tables are typed in the same style as the text and are denoted by numerals at the top. Photographs and drawings, placed appropriately in the text, should be clear, precise and suitable for reproduction. Drawings should be created in Word or Corel.

Citation in the Text

Citation in the text must be uniform. When citing references in the text, use the reference number set in square brackets from the Reference list at the end of the article.

Footnotes

Footnotes are given at the bottom of the page with the text they refer to. They can contain less relevant details, additional explanations or used sources (e.g. scientific material, manuals). They cannot replace the cited literature.
The article should be accompanied with a cover letter with the information about the author(s): surname, middle initial, first name, and citizen personal number, rank, title, e-mail address, and affiliation address, home address including municipality, phone number in the office and at home (or a mobile phone number). The cover letter should state the type of the article and tell which illustrations are original and which are not.

Address of the Editorial Office:

Enriched Publications Pvt. Ltd.
S-9,IInd FLOOR, MLU POCKET,
MANISH ABHINAV PLAZA-II, ABOVE FEDERAL BANK,
PLOT NO-5, SECTOR -5, DWARKA, NEW DELHI, INDIA-110075,
PHONE: - + (91)-(11)-45525005

Journal of Water Resources and Civil Engineering Technology

SUBSCRIPTION FORM

SUBSCRIPTION PRICES

India	Institutional	Individual
Print	3000 INR ☐	2000 INR ☐
Print + Online	4000 INR ☐	3000 INR ☐
Online	1500 INR ☐	800 INR ☐
Rest of the world	**Institutional**	**Individual**
Print	300 USD ☐	200 USD ☐
Print + Online	400 USD ☐	300 USD ☐
Online	200 USD ☐	150 USD ☐

Contact Person : _____

Designation: _____

Institution Name:_____

Address :_____

_____

City : _____ Pin : _____State :_____

Tel : _____Fax : _____ Email :_____

PAYMENT OPTIONS

☐ Cheque / DD is enclosed in favour of **" Apex Subscription Pvt. Ltd."** Payable at Mumbai.

Amount : _____

Cheque / DD No : _____ Dated : _____ Drawn on Bank

_____

☐ **NEFT / RTGS :**

Beneficiary Name : Apex Subscription Pvt. Ltd.

Bank Name : HDFC Bank Ltd, BRANCH : Goregaon (East),

Bank A/C No : 02122320004035, IFSC Code: HDFC0000212

Note : For more subscription detail follow the link www.apexsubs.com

Editorial Office
Enriched Publications Pvt. Ltd
S-9, IInd Floor Above Federal Bank,
Plot No-5, Sector-5, Dwarka, New Delhi- 110075,
Phone: - + (91)-9892508945
Email : sales@enrichedpublications.com
Website : www.enrichedpub.com

Subscription Manager
APEX SUBSCRIPTION PVT LTD.
304, De-Elmas, Sonawala Cross Road 2,
Goregaon (East) Mumbai - 400063.
Tel : +91-022-26853114/5 Fax : 022-26853116
Email : enquiry@apexsubs.com
Website : www.apexsubs.com

Note